Natural H2 exploration: tools and workflows to characterize a play

Dan Lévy, Vincent Roche, Gabriel Pasquet, Valentine Combaudon, Ugo Geymond, Keanu Loiseau, Isabelle Moretti

Science and Technology for Energy Transition **78**, 27 (2023)

https://doi.org/10.2516/stet/2023021

Available online at:
stet-review.org

REVIEW ARTICLE OPEN ACCESS

Natural H_2 exploration: tools and workflows to characterize a play

Dan Lévy[1,*], Vincent Roche[2,3], Gabriel Pasquet[2], Valentine Combaudon[2,4], Ugo Geymond[1,4], Keanu Loiseau[2,5], and Isabelle Moretti[2,3]

[1] Institut de physique du globe de Paris (IPGP), CNRS, Université Paris Cité, 1 rue jussieu, 75005, Paris, France
[2] Laboratoire des Fluides Complexes et leurs Réservoirs (LFCR), E2S UPPA, Université de Pau et des Pays de l'Adour, Avenue de l'université, 64000 Pau, France
[3] Institut des Sciences de la Terre de Paris (ISTeP), Université Pierre et Marie Curie, 4 place Jussieu, 75005 Paris, France
[4] IFP Energies Nouvelles (IFPEN), 1-4 Av. du Bois Préau, 92852 Rueil-Malmaison, France
[5] CVA-Engineering, 2 Rue Johannes Kepler, 64000 Pau, France

Received: 15 June 2023 / Accepted: 1 August 2023

Abstract. Natural dihydrogen (H_2) exploration is now active in various countries, but tools and workflows that help to characterize prospective zones are still poorly defined. This review paper is dedicated to share our experience in characterizing H_2 plays based on exploration efforts carried out in many countries in Europe, North and South America, Africa, and Oceania between 2017 and 2023. We decided to focus on onshore exploration where three main reactions are generating H_2: (i) redox reactions between Fe^{2+} and H_2O, (ii) radiolysis of water and, (iii) organic late maturation where H_2 comes from hydrocarbons. This leads to classify the H_2 generating rocks (H_2_GR) into four types that seem us the more likely to be of economic interest: basic and ultrabasic rocks of oceanic/mantellic affinity (H_2_GR1), iron-rich bearing sedimentary and intrusive rocks, (H_2_GR2), radioactive continental rocks (H_2_GR3) and organic matter-rich rocks (H_2_GR4). For the pre-fieldwork, the workflow aims to target new promising areas for H_2 exploration. Cross-referencing the presence of H_2_GR in the basement, classical geological-hydrodynamic features (fault, water source), and already-known H_2 occurrences at the surface remain essential but should be accompanied by remote sensing analyses to detect possible H_2 occurrences. For the fieldwork, the focus is made on gas and rocks. A discussion is led concerning the importance of punctual measurements and long-term monitoring of gas seepages, that allow to conclude on dynamics of H_2 leakage from depth through space and time. For the post-fieldwork, we present the most useful analytical tools to characterize H_2 gas seepages and the suspected H_2_GR. The critical parameters to estimate the H_2 potential of a rock are the content in Fe^{2+}/Fe_{tot} (H_2_GR1 and H_2_GR2), the content of radioactive elements U, Th, K (H_2_GR3), and the total organic content (H_2_GR4). The hydrogen exploration is in its infancy and all the profession is attempting to define an automated and fast workflow. We are still far away from it due to a lack of data, yet this review presents a practical guide based on the current knowledge.

Keywords: Natural H_2, Exploration, H_2 generating rocks, H_2 play.

1 Introduction

Dihydrogen (H_2) is an important molecule used in the chemical industry as well as in the mobility sector. But, the main processes of producing H_2 are based on the use of hydrocarbons and coals which emit CO_2. The green hydrogen formed by electrolysis from green electricity is also considered as an important player in the future H_2 market because of its lower carbon impact. However, since the discovery in 2007 (Diallo *et al.*, 2022) of an almost pure H_2 accumulation in a well in Mali, the idea that natural hydrogen could be considered as a primary energy without greenhouse gases emission is emerging. Yet, the discovery of this well has been fortuitous, and at that time, the natural H_2 exploration was at its early stage (Smith *et al.*, 2005).

Since then, a lot of new studies were launched based on the multiple works on serpentinization, a process known to produce H_2 in the mid-oceanic ridges (MOR; Klein *et al.*, 2017; Mével, 2003; Proskurowski *et al.*, 2006) and new evidence of H_2 presence in other geological contexts (Boreham *et al.*, 2021; Larin *et al.*, 2015; Lefeuvre *et al.*, 2021; Prinzhofer *et al.*, 2018, 2019; Zgonnik *et al.*, 2015). It has been 10 years since H_2 was actively explored and the acquired data and experience have only been rising (Truche *et al.*, 2020). Whereas several reviews appear on defining the different sources of H_2 (Worman *et al.*, 2020; Zgonnik,

* Corresponding author: dlevy@ipgp.fr

2020), it is not always relevant in terms of risks taken to produce natural H_2 (Gaucher *et al.*, 2023). Here, we discuss exploring H_2 onshore which is consistent with H_2 production. Moreover, we decided to focus on the first steps of the exploration and we do not take into consideration the seals and reservoirs allowing the accumulation of H_2.

Based on our experience of H_2 exploration in many regions of the world (France, Italy, Iceland, Brazil, Republic of Djibouti, Ethiopia, South Africa, Namibia, Bolivia, and Australia), we propose tools to efficiently explore this new resource divided into four steps: (i) pre-fieldwork consisting on spotting the H_2 hot spots thanks to existing literature and remote sensing techniques, (ii) fieldwork during which we acquire *in situ* gas data and samples of potential rocks of interest, (iii) post-fieldwork during which we perform laboratory analyses on gas and rocks, and (iv) discussion of results to better characterize a play.

2 Pre-fieldwork

Pre-fieldwork consists in reviewing all available data that may provide information indicating the presence of H_2 (*i.e.*, seepage or measurement of H_2 in water sources or wells generally done for another purpose) and/or the presence of H_2-generating rocks (H_2_GR) at various scales (*e.g.*, country, basin) to select and define a prospective area. We first present a review of the lithologies as well as minerals favorable to the H_2 generation to locate the main areas of interest. Then we present the different tracers indicating the presence of H_2 and we propose a new approach based on remote sensing to investigate H_2 occurrences in Sub-Circular Depressions (SCDs). Finally, we present a workflow combining all these tools.

2.1 Lithologies of interest for H_2 generation

To target the locations where H_2 can be present in abundance, it is important to first define the processes that generate H_2. However, as previously mentioned, we will not emphasize the processes occurring offshore or in geothermal areas. Indeed, offshore will not be immediately economic, and in geothermal areas, even if the H_2 potential exists (Combaudon *et al.*, 2022; Leila *et al.*, 2021; Pasquet *et al.*, 2021), the exploration workflow is close to the classical one used by the industry to find hot steam. Moreover, the existence of a law allowing exploration and production of H_2 as a natural resource is also mandatory to select potential areas of interest but it will not be discussed in this paper, and fortunately, the list of these countries is getting progressively longer.

Here, we focus on the three following main processes producing H_2: (i) redox reaction between Fe^{2+} and H_2O that takes place during aqueous alteration like serpentinization or hematization, (ii) radiolysis of H_2O and (iii) organic maturation.

(i) For many years, hydrogen was considered to be mainly generated by the reaction of serpentinization which is the process of aqueous alteration of peridotite into serpentinite, where the olivine is altered into serpentine and magnetite produces H_2. This process takes place mainly in the MOR at temperatures between 150 °C and 350 °C (Klein *et al.*, 2013) and also onshore on the ophiolites at lower temperatures (Etiope *et al.*, 2011; Neal and Stanger, 1983; Vacquand *et al.*, 2018). If we simplify the reaction of alteration, the serpentinization process can be considered a redox reaction where Fe^{2+} in olivine is oxidized into Fe^{3+} in magnetite while reducing water into H_2:

$$2Fe^{2+}O + H_2O = {Fe^{3+}}_2O_3 + H_2. \quad (1)$$

Redox reactions are present in many alteration processes that are now considered favorable for the production of H_2, like the alteration of Banded Iron Formations (BIFs; see *e.g.* Geymond *et al.*, 2022), containing magnetite that can be altered into maghemite and/or hematite. These rocks are mainly present in cratonic areas and recent experimental alteration studies showed that such a process could occur at low temperatures (Geymond *et al.*, 2023).

(ii) Radiolysis involves the natural radioactive decay of the elements such as uranium, potassium, and thorium. In this case, radiolysis leads to the dissociation of water molecules, if present, into H and OH. This mechanism is usually invoked in the Archean and Proterozoic domains where rocks contain uranium-, potassium- and thorium-rich minerals.

(iii) It was recently shown that the late pyrolysis of organic matter (especially coal and shaly coal) also generates H_2 that may remain as a free gas (Horsfield *et al.*, 2022; Mahlstedt *et al.*, 2022; Suzuki *et al.*, 2017).

Other processes like degassing of deep H_2 (Zgonnik, 2020), and mechanoradical (Hirose *et al.*, 2011), could also contribute to the generation of H_2 but we would not mention it because it is currently difficult to trace it in the context of H_2 exploration. Moreover, no company is targeting volcanic H_2, which may come from the decomposition of H_2S (Zgonnik, 2020), and it will not be addressed here.

These three aforementioned processes lead us to divide the main H_2_GR into four main groups presented in Figure 1:

- H_2_GR1: Basic and ultrabasic rocks from mantellic/oceanic affinity (*e.g.*, peridotite, gabbro, basalt); their hydrothermal alteration generates H_2 through different reactions like the serpentinization process.
- H_2_GR2: Iron-bearing rocks (sedimentary rocks such as banded iron formations (BIFs), intrusive rocks such as biotite-rich granites ...) that generate H_2 through oxido-reduction processes during aqueous alteration.
- H_2_GR3: Radioactive rocks that may generate H_2 through radiolysis, in the presence of H_2O.
- H_2_GR4: Organic-rich rocks such as coal, shale, and coaly shale that generate H_2 at high temperatures. It is the only group generating H_2 independent of H_2O.

In addition, these groups contain various minerals involved in the reactions producing H_2. We note that a single mineral can make the required reaction but the

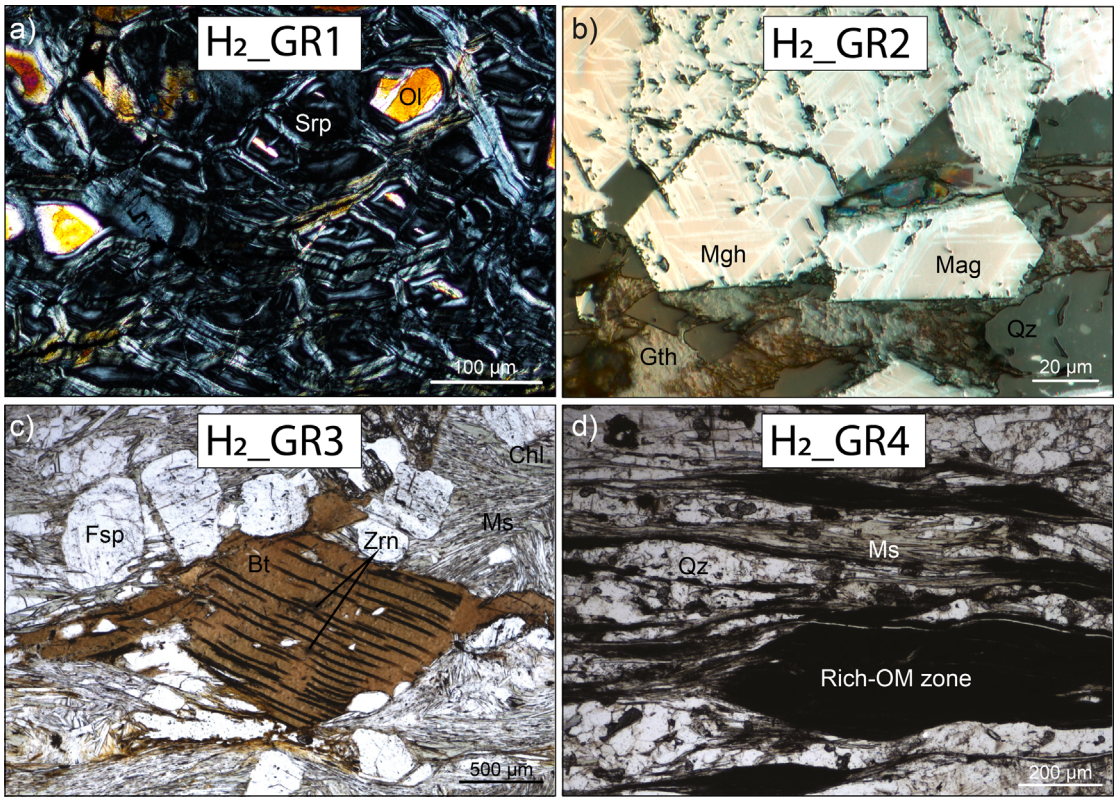

Fig. 1. Optical micrographs of thin sections of four different H_2 generating rocks (H_2_GR) belonging to categories H_2_GR1-4 showing different mineral assemblages in Cross-Polarized Light (CPL), Plane Polarized Light (PPL), and Reflected Light (RL). (a) a serpentinite (CPL) where olivine was altered into serpentine. (b) a BIF (RL) with a replacement of magnetite into maghemite, (c) a granite with biotite and zircon (PPL), and (d) an organic matter-rich rock (PPL). Bt: biotite, Fsp: feldspar, Mag: magnetite, Mgh, maghemite, OM: organic matter, Ms: muscovite, Ol: olivine, Qz: quartz, Srp: serpentine, Zrn: zircon.

Table 1. H_2 generating rocks (H_2_GR) and their related minerals of interest for H_2 generation.

Geological context	Oceanic rocks		Continental rocks	
H_2_GR type	H_2_GR1: Oceanic lithosphere, Ophiolites	H_2_GR2: Iron-bearing rocks (BIF, greenstone belts)	H_2_GR3: Granitic and sedimentary rocks	H_2_GR4: Organic-rich rocks (shale, coal)
Process	Redox reactions	Redox reactions	Radiolysis	Late maturation
Minerals of interest	Olivine, Pyroxene, Amphibole, Chlorite, Serpentine, Magnetite, Pyrrhotite	Olivine, Pyroxene, Amphibole, Chlorite, Serpentine, Magnetite, Garnet, Siderite, Pyrrhotite	U-minerals, Micas, K-feldspars, Clay minerals	Organic matter (kerogens)

associated minerals forming the rock can catalyze or inhibit these reactions. Thus, it is important to characterize the mineralogical assemblage. The minerals are presented in Table 1 and the reaction paths for redox reactions are given in Appendix A.

Figure 2 shows four maps that we synthesized based on the worldwide distribution of H_2_GR introduced previously. The first map indicates the spatial surface distribution of H_2_GR1 consisting of slices of oceanic lithosphere onto the continent (named ophiolites) that could undergo serpentinization. H_2 measurements (green dots) potentially related to this process are located in several places related to ophiolites/peridotitic massifs such as in Spain (Ronda, Etiope *et al.*, 2016), Oman (Chavagnac *et al.*, 2013; Neal and Stanger, 1983), Turkey (Chimaera, Etiope *et al.*, 2011), Philippines (Zambales, Abrajano *et al.*, 1988), New

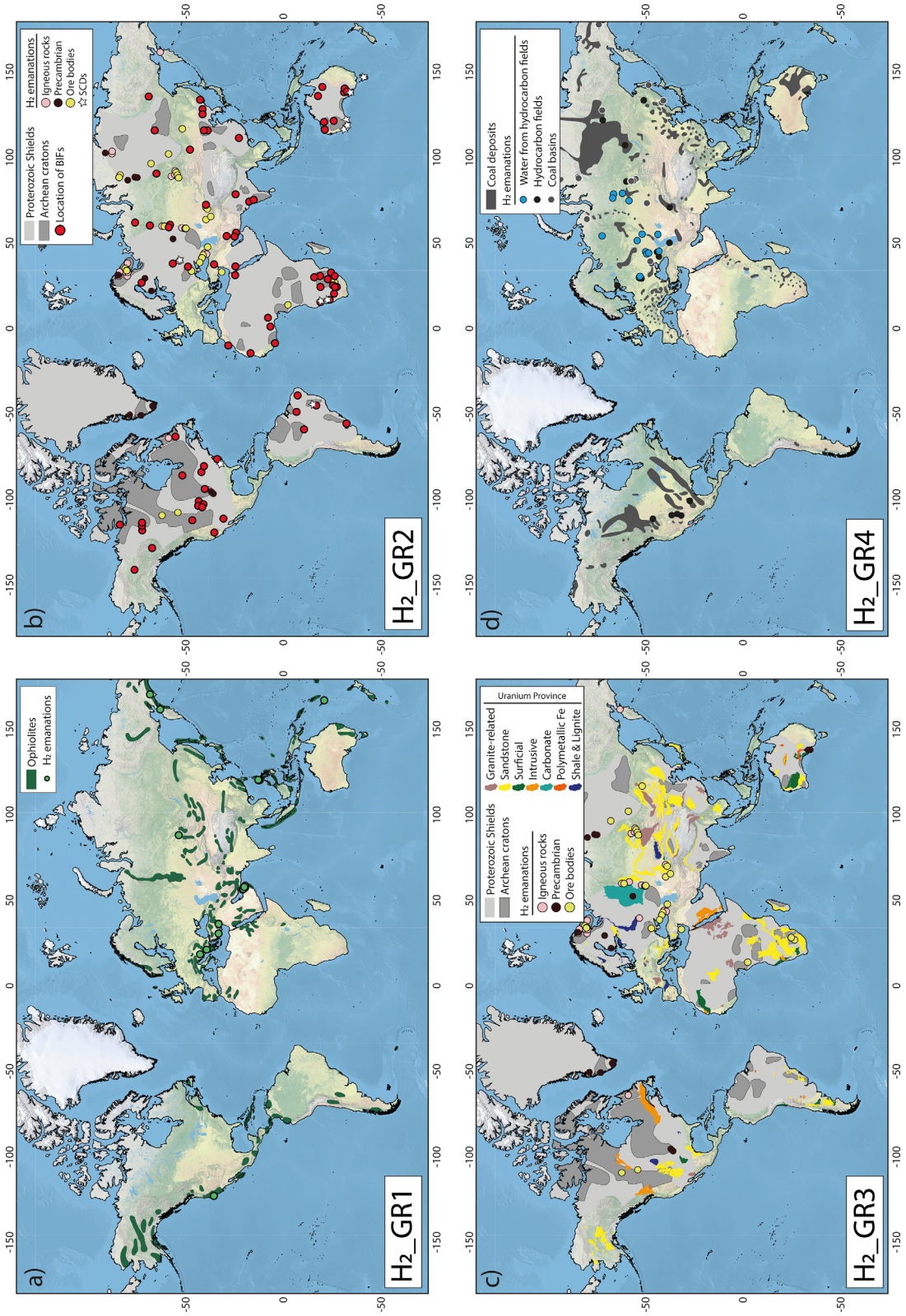

Fig. 2. Global presence of H_2_GR indicated on a topographic map (ESRI National Geographic USA Topo Maps). (a) The spatial distribution of ophiolites from Vaughan and Scarrow (2003). (b) Cratonic and proterozoic zones (Furnes *et al.*, 2015) combined with fairy circles location (Larin *et al.*, 2015; Zgonnik *et al.*, 2015) and BIFs (Aftabi *et al.*, 2021). (c). Distribution of uranium provinces differentiated by lithologies from the International Atomic Energy Agency (2021). (d) Spatial distribution of coal deposits. Note that dots from the study of Zgonnik (2020) correspond to H_2 detections in various environments at concentrations >10 vol.%.

Caledonia (Deville and Prinzhofer, 2016), and in the Balkans (Lévy *et al.*, 2023). Even if the ophiolites represent small areas on the land scale compared to MORs, they represent a huge potential for serpentinization and therefore H_2 generation.

Figure 2b shows the location of H_2_GR2 that corresponds mainly to BIFs (red dots) occurrences associated with cratonic areas, including also Proterozoic rocks. At first glance, there is a correlation between these old rocks, H_2 detections, and SCDs, some of which are proven to be related to H_2 emanations (Geymond *et al.*, 2022; Moretti *et al.*, 2021a). Indeed, all these indicators are often localized close to BIFs (Brazil, Australia, the United States, Namibia, and Russia). But, other lithologies (igneous rocks, Precambrian rocks, or associated with ore bodies) present mainly in Archean and Proterozoic rocks are also associated with H_2. For example, hydrothermal alteration of peralkaline intrusions (*e.g.*, Strange Lake in Canada, Lovozero, and Khibiny in Russia) may lead to H_2 generation (Truche *et al.*, 2021). In such a context, the Fe^{2+}-bearing amphibole is considered as a reducer, and water is an oxidant (1). Other mine areas look also promising as evidenced by Boreham *et al.* (2021) and Malvoisin and Brunet (2023).

Figure 2c combines the uranium provinces and the Archean and Proterozoic rocks. The H_2_GR3 corresponds therefore to the rocks that can generate H_2 from the radiolysis of water. Such a process may be present everywhere but with different intensities. At large scale, there are some overlaps with the Archean and Proterozoic domains because these rocks contain various uranium- and thorium-rich minerals. Further, the best way to identify the radiolysis mechanism is probably related to the presence of He, because crustal He could only be generated by radioactivity. They are sometimes found together such as in Australia (Leila *et al.*, 2022), South Africa (Karolytė *et al.*, 2022), and the USA (Halford *et al.*, 2022).

Finally, Figure 2d indicates the spatial distribution of the coal resources. There is no clear correlation between the H_2 measurements (HC fields, water from HC fields, and coal basins following the classification of Zgonnik (2020) and coal deposits yet. This implies that H_2 potential is probably underestimated in the coal deposit areas.

In general, it is better to have more than one H_2_GR in the selected country to increase the probability of success, and/or a large zone with a potential H_2_GR. For example, Australia, the USA, Brazil, and Russia have at least three types of H_2_GR.

2.2 Indicators of the H_2 presence

After locating the potential zones of interest for H_2 generation, different methods can be used to focus on zones that are targets for H_2 production. First, work on finding data in the available literature has to be done. Indeed, some interesting information can indicate the direct presence of H_2 in wells or gas seeps. If no data on the H_2 presence is available, it is possible to map the different gas emissions (dissolved or not) in boreholes, free gas vents, or as bubbles whatever the flux.

2.2.1 Boreholes and seismic data

Many discoveries of H_2 occurrences were made after drilling campaigns for Oil and Gas (O&G), mining, or hydrogeological purposes (Fig 3a). In the Yorke Peninsula (Australia), H_2 was noted for the first time in the early 20th century after the drilling of an oil exploration well, the Minlaton Oil Bore (Ward, 1933) which reached 548 m in depth. Similarly, in Kansas (USA), eight oil exploration wells were drilled in the 1980s. Scott#1 (677 m) and Heins#1 (770 m) wells gave unusual free gas compositions with an average H_2 of 29 and 37 vol.%, respectively (Coveney *et al.*, 1987; Guélard *et al.*, 2017). In more recent exploration wells, H_2 is often not mentioned but it makes sense to revise all the available literature. For example, Zgonnik (2020) compiled hundreds of sites where H_2 has already been measured based on archive data (Fig. 2). In Australia (around Adelaide), in the USA (Kansas), and in Spain, the first natural H_2 exploration licenses have been taken around historic wells with H_2-rich gases. Thus, well reports and associated survey reports must be examined carefully to derisk large areas. Here, H_2 can be directly mentioned, or in certain cases, hidden in "undefined inflow gases". It is important to mention that H_2 may also be generated by causing oxidation.

The gas chimneys and pockmarks (Fig. 3b) are also proof of gas dismigration. Well-imaged on high-resolution 3D offshore seismic data, they could be also visible onshore, even on 2D seismic lines. Gas chimneys are rooted in the basement and have been, for instance, described in Australia (Leila *et al.*, 2022). Such features make it possible to be confident of the existence of a gas flow at depth, even if the gas chemistry cannot be extrapolated.

Geophysical data can be acquired to detect the presence of dense and/or magnetic H_2_GR like mantellic rocks and BIF, from gravity (Lefeuvre *et al.*, 2021) and magnetic susceptibility measurements respectively.

2.2.2 Free gas vents

There are a few surface markers that allow us to recognize H_2 emanations. If the concentration is large enough, self-ignition of H_2 can occur, with an invisible flame. When blended with CH_4, the flame can be observed. Such a permanent fire is a curiosity often reported as in Chimaera in Turkey. This "flaming rock" has been known since at least 2000 AD, and recent analyses revealed H_2 concentrations up to 11 vol.% in the free gas mixture whereas CH_4 concentrations reach ~87 vol.% (Etiope *et al.*, 2011). In areas of geothermal activity, fumaroles have also to be targeted (Fig 3c, South Lipez, Bolivia; Moretti *et al.*, 2023). For example, H_2 contents ranging from 0.2 to 4.6 vol.% and around 0.7 vol.% were measured in H_2O-rich free gases rising to the surface at around 95 °C in the Larderello geothermal zone (Leila *et al.*, 2021) and in the Asal rift (Pasquet *et al.*, 2021) respectively.

2.2.3 Dissolved gases and bubbling water:

Dissolved gases and bubbling water reflect the pathway of fluids within the crust and therefore testify and offer

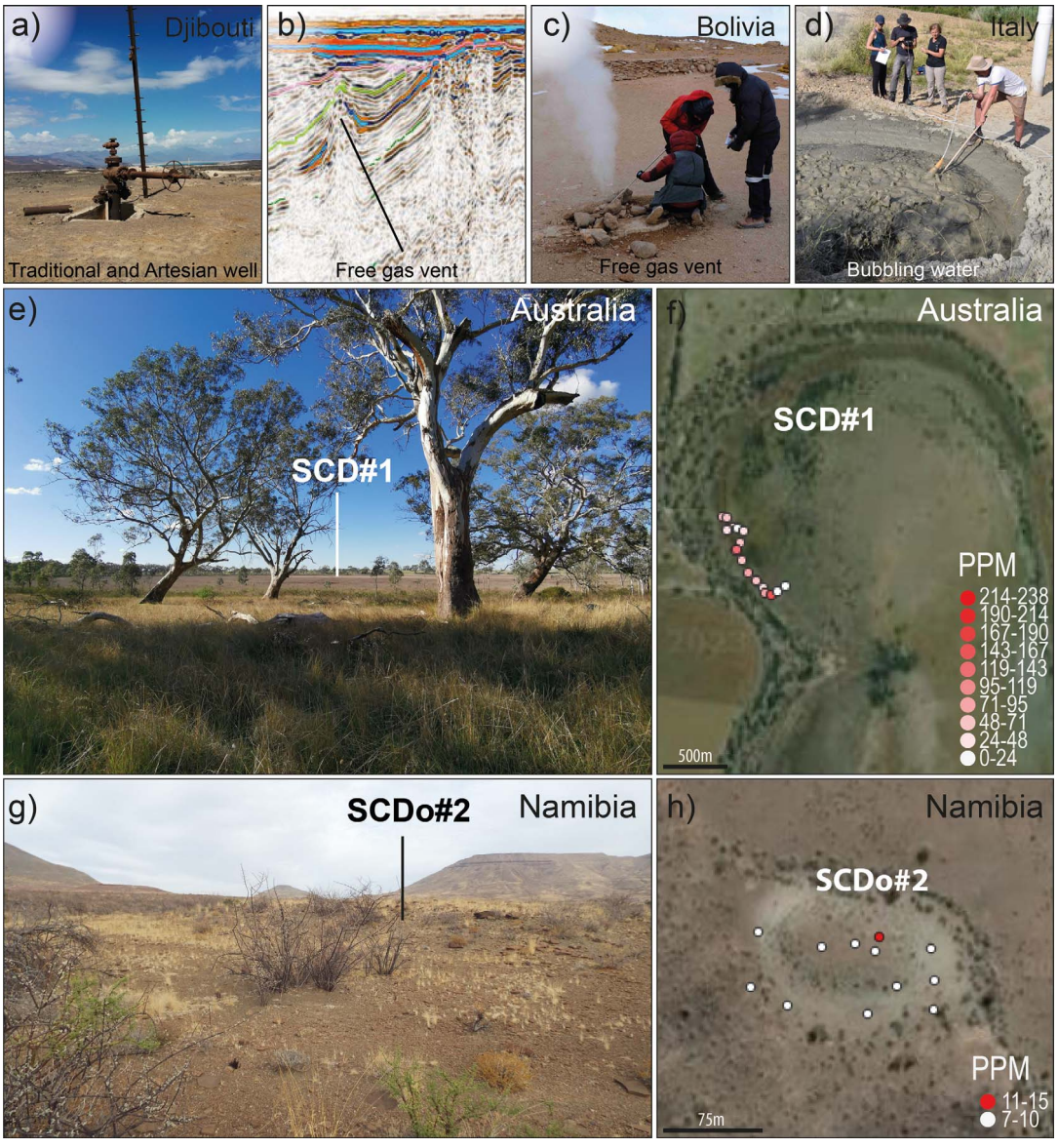

Fig. 3. H_2 source types and associated photographs during field trips: (a) Borehole in the Republic of Djibouti. (b) Gas chimney on seismic data. (c) Free gas vent in Bolivia. (d) Bubbling water in Italy. SCD in (e, f) Australia and (g, h) in Namibia. See Appendix B for coordinates.

potential proxies of water-rock interaction processes (Fig. 3d). The H_2 may first be dissolved in the aqueous phase since high pressure increases the solubility of H_2 (Lopez-Lazaro *et al.*, 2019). A decrease in pressure near the surface triggers H_2 exsolution, favoring the bubbling in spring waters. This is observed for instance in the ophiolitic contexts that currently get serpentinized. H_2-rich bubbling is reported in New Caledonia (up to 36 vol.%), Oman (up to 87 vol.%), the Philippines (up to 59 vol.%), and the Balkans (up to 84%) (Lévy *et al.*, 2023; Randazzo *et al.*, 2021; Vacquand *et al.*, 2018). In this kind of spring, the water is usually hyperalkaline, with a pH higher than 9 often related to the serpentinization process. So, the presence of bubbles in water could be a good candidate to find natural hydrogen when H_2_GRs have been identified in the area. Before going to the field, therefore it is recommended to identify these thermal manifestations (*e.g.*, fumaroles, springs).

2.2.4 The special case of SCDs

SCDs are an important marker of H_2 flow in the soils (Figs. 3e–3h). They have been first described and linked to H_2 presence in Russia (Larin *et al.*, 2015) and then targeted all over the world (in the USA, Zgonnik *et al.*, 2015; Mali, Prinzhofer *et al.*, 2018; Brazil, Prinzhofer *et al.*, 2019; Moretti *et al.*, 2021b; and Australia, Frery *et al.*, 2021; Moretti *et al.*, 2021a). However, all the SCDs are not related to H_2 emanations. The first publications were only based on the geometric parameters of the SCDs

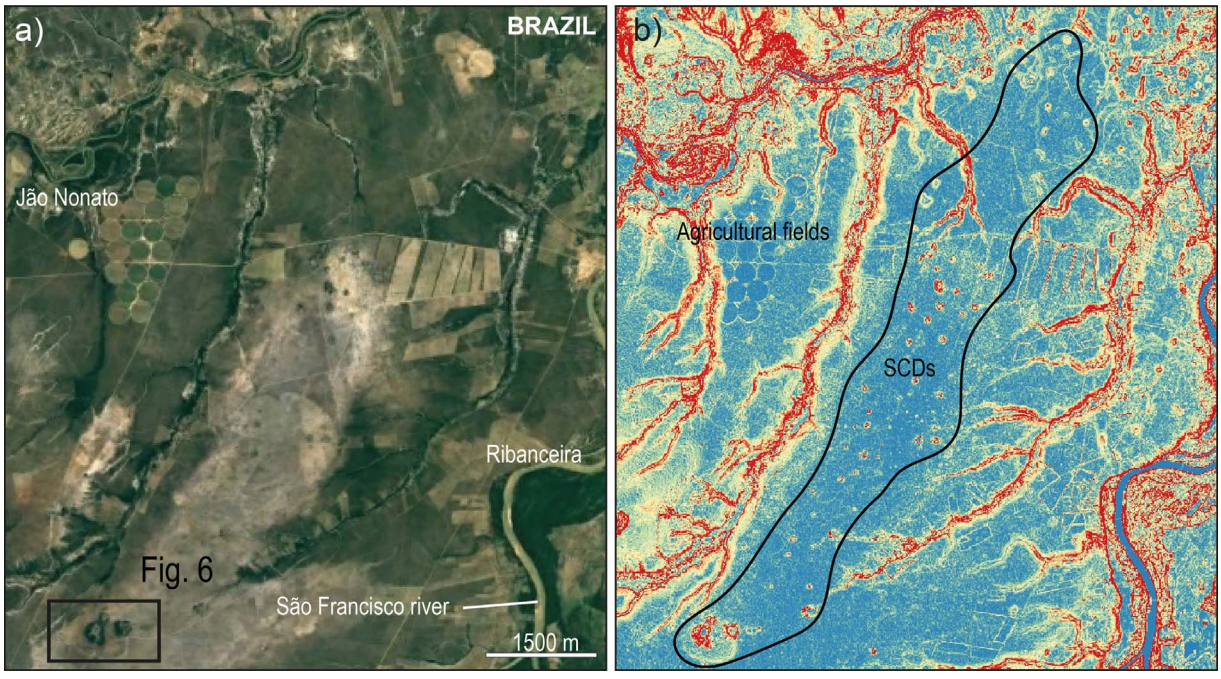

Fig. 4. (a) Satellite image and (b) slope map of the Minas Gerais region (Brazil) showing the SCDs. The two SCDs in the black rectangle have been monitored for 2 years (Moretti *et al.*, 2021b; Prinzhofer *et al.*, 2019). The SCDs are located in the small hills between the rivers. The slope is deduced from the Digital Elevation Model (DEM) highlighting also the rivers, the agricultural activity, and the SCDs. Note that SCDs have a rather flat bottom and a positive relief around them. See Appendix B for coordinates.

(size, depth, density). Here, we present the recent improvements in the detection of H_2-related SCDs.

2.2.4.1 Morphological characteristics

Size, slope, and depth. The SCDs have a circular and/or ovoid feature shape in the landscapes (Figs. 3e and 3g) and may be easily identified from satellite images such as Google Earth images (Figs. 3f and 3h). In rare cases, the shape is a dome-like structure (SCDo) and may reach also a few meters in height. When present in an area, the SCDs are numerous often exceeding one hundred. Depending on the location, the size of the circle generally varies from 25 m to 1 km in diameter and a few meters in depth. Moretti *et al.* (2021a) used a statistical approach to the size of the circle in terms of equivalent diameter which corresponds to a perfect circle diameter having the same area as the SCD. They showed also a relationship between this equivalent diameter and the depth that is around 1% and that the slope at the border of the depression is usually less than 3%. Thus, slope mapping may be used to identify rapidly the SCDs. For example, Figure 4 indicates the differences between these natural structures (central part), the anthropic ones (perfect circles NW), and the rivers in the Minas Gerais region in Brazil. In this area, 86 SCDs have been reported with an average depth/diameter of 0.013 (Moretti *et al.*, 2021a). These three characteristics (depth, depth/diameter, and slope) allow us to differentiate the karst-related dolines from the SCDs even if the size could be similar.

In parallel, other SCDs could be observed from satellite images although they happen to be not related to any H_2 emanations when we go further on the field (Fig. 5). Additional criteria might help when the differences from the satellite images are not straightforward with the H_2-related SDCs. In the case of Namibia and South Africa, some depressions are characterized by both ovoid and circular shapes, exhibiting a gap of vegetation and are only a few meters deep but are probably related to wind activity in these desert areas and/or to termite activity (Tinley, 1971), even though other processes are not totally excluded (*e.g.*, plants with poisonous Euphorbia plants, Theron (1979) or rodent activity, Cox (1987)). Some of them are located in the northern part of South Africa, in the low and high topographic zones, and measure only a few meters in diameter (Fig. 5a). They are also numerous in Namibia, and are easily differentiated by their small sizes and their regular hexagonal patterns with a clear degree of spatial ordering. Others are located in the desert in the southeastern part of Namibia and related to dunes activity favored by wind flow blowing (Fig. 5b). The size of the depressions here is a few hundred meters in diameter and tens of meters in depth. Thus, the systematic anisotropy of the depth and slope with regard to the wind direction is a criterion that has to be checked.

2.2.4.2 Multispectral anomalies

To better characterize the H_2-related SCDs, Moretti *et al.* (2022) have recently proposed a proxy based on Landsat Multispectral Images through their Normalized Difference Vegetation Index (NDVI) and Soil Adjusted Vegetation

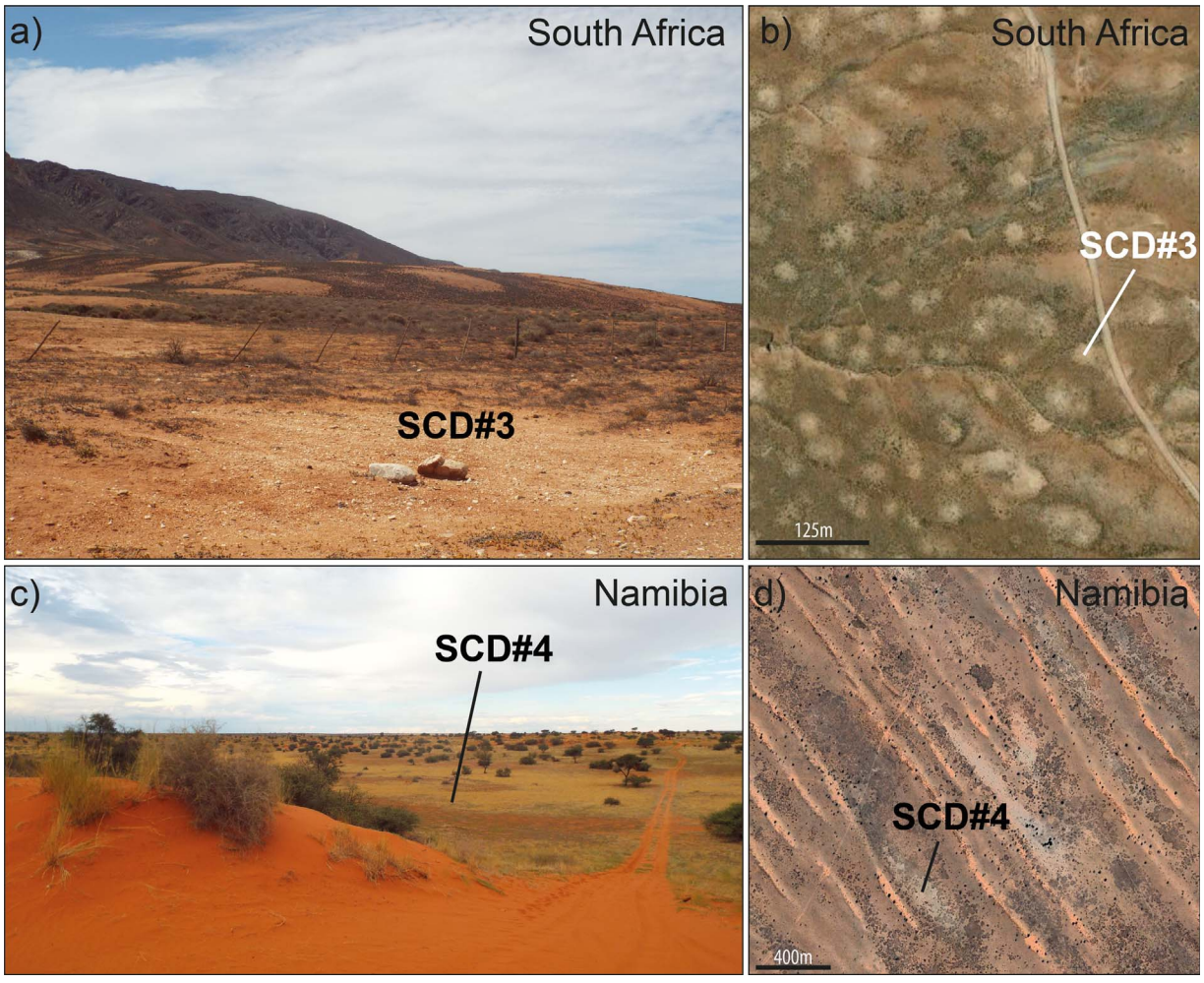

Fig. 5. Sub-circular structures without H_2 emanations and without vegetation observed (a, c) on the field and (b, d) on Google Earth. See Appendix B for coordinates.

Index (SAVI) combined with the coastal aerosol band. They observed that, in the case of H_2 seepage, the vegetation evolves within the circular structure ranging from scarce in the center to healthy toward the edge. Such a particular evolution allows them to discriminate H_2-emitting structures from other depressions. Figure 6 shows indexes that highlight the SDCs from satellite data on the Brazilian structure studied by Prinzhofer *et al.* (2019) and (Moretti *et al.*, 2021b).

Further, other indexes may be used to differentiate the SDCs from the rest like the gamma-ray anomalies described in Brazil around the SCDs (Rigollet and Prinzhofer, 2022) or the ferrous mineral ratio that can also be estimated from the Landsat image. This latter ratio can be used to detect iron-bearing rocks outcropping at a regional scale.

2.2.4.3 Evolution of SCDs with time

Other data could be also interesting to evaluate the change of SCDs over time. Google Earth satellite images may be watched through time and the onset of SCDs has been already observed in Russia (Larin *et al.*, 2015) as well as in the USA (Zgonnik *et al.*, 2015). In areas where agricultural activity is intense, it can be noted that the efforts of farmers to cultivate the SCDs areas failed. A few years later, the vegetation anomaly related to the SCDs comes back. Further, in the same way, the Landsat images may be used to characterize SCDs evolution. In some specific regions, the timing of the vegetation indexes acquisition above the SDCs could influence the interpretation. Indeed, both NDVI and SAVI depend on rainfalls or snow precipitations. If those precipitations are important, the indexes can change drastically. This is particularly the case for cold areas such as Russia (Fig. 7). Here, snow is present and covers the SCDs a part of the year. It is therefore important to show the related RVB image before interpreting the results. But, in our experience, the SCDs related to gas emanations are always visible. Finally, the study of the soil vertical displacement using high-resolution DEM and/or interferometry would be also interesting to ensure that

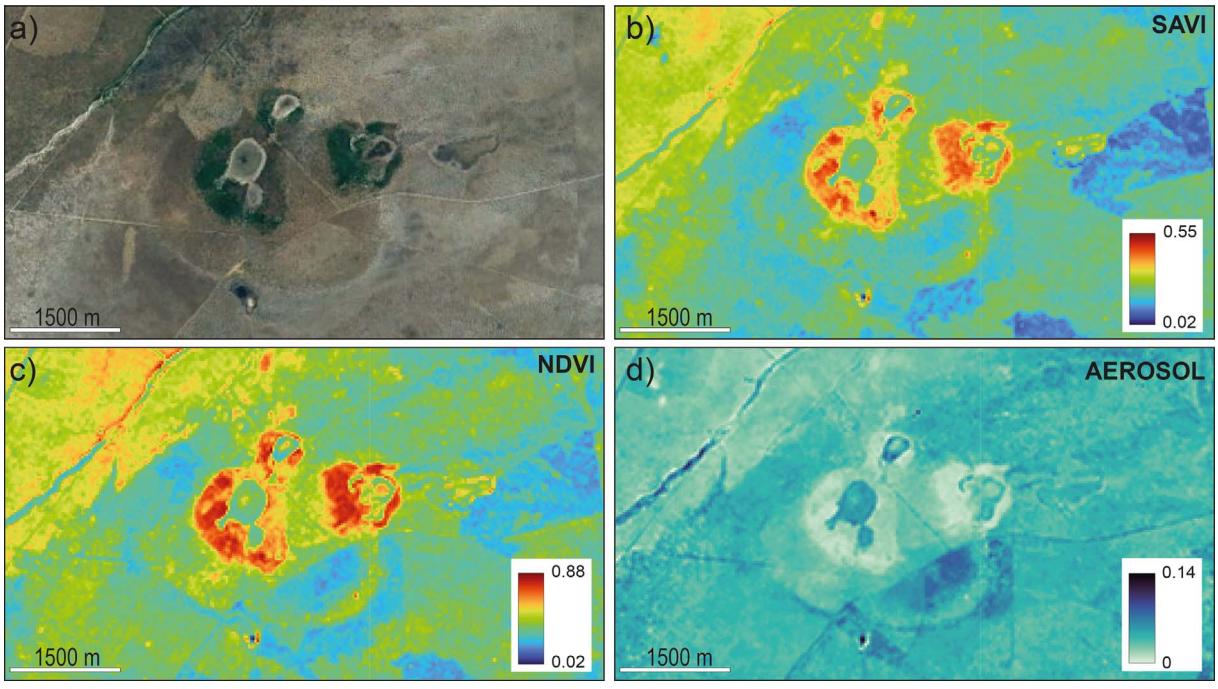

Fig. 6. SCDs in Brazil (see location Fig. 4). (a) Satellite Google Earth image. (b, c) Vegetation Indexes deduced from the Landsat infrared images showing healthy vegetation in red around SCDs. Note that they highlight three major H_2-emitting structures as well as a larger one that encompasses them. (d) Aerosol index showing low concentrations in light blue around SCDs.

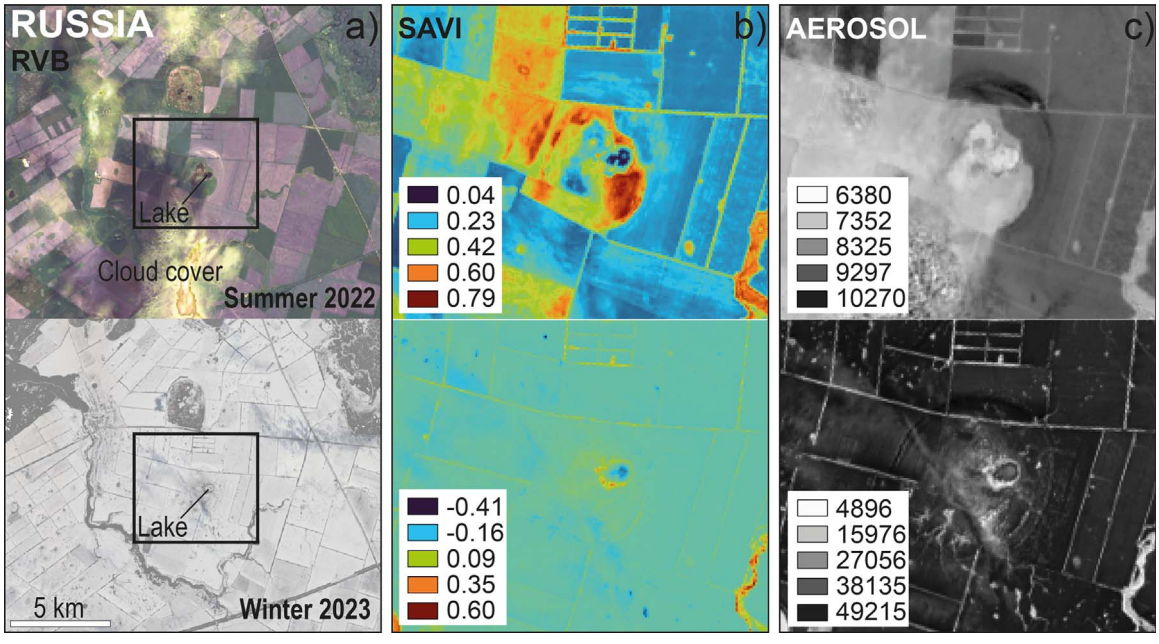

Fig. 7. (a) Comparison of the expression of SCDs in Russia in summer and winter and (b, c) zoom in the black square on SAVI and aerosol data. See Appendix B for coordinates.

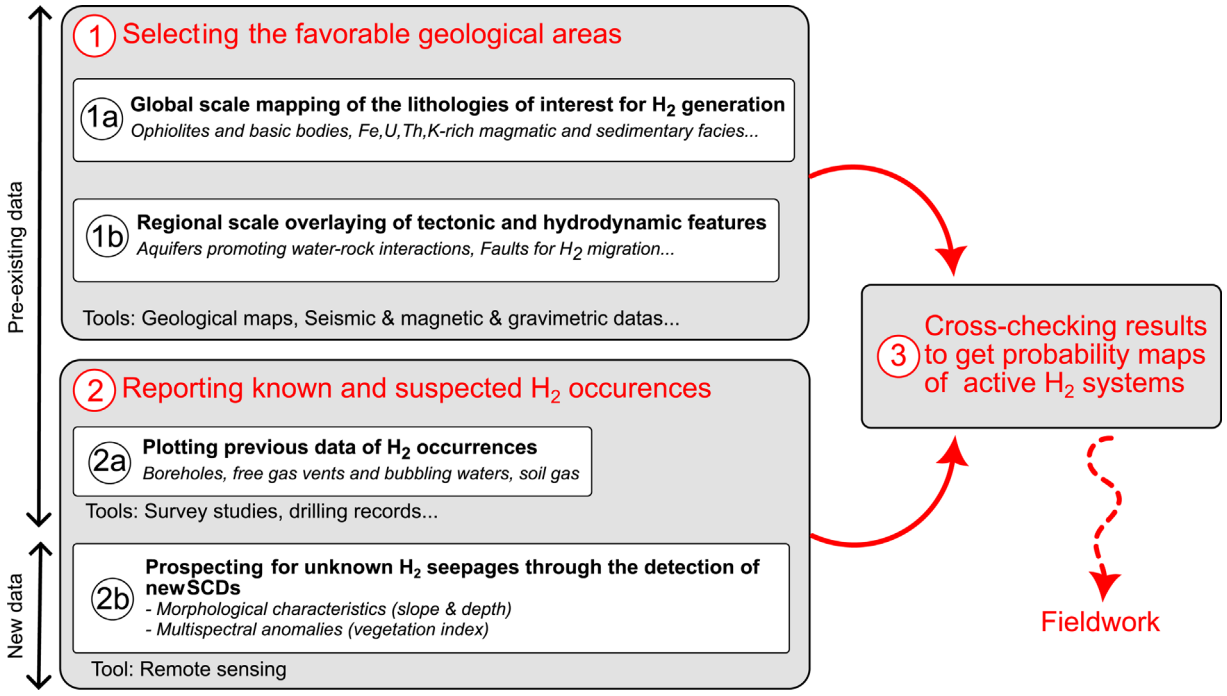

Fig. 8. Workflow to target potential H_2-rich locations and to organize field acquisitions.

the structure is still active, however, there is no publication on such a technique.

2.3 Workflow for the pre-fieldwork

Two points are important to get a probability map of H_2 and to define a pre-field workflow: (1) selecting the favorable geological areas for H_2 generation combining potential H_2_GR and subsurface data and (2) reporting known and suspected H_2 occurrences (Fig. 8). In addition, if the area of interest is located on an ophiolite, hyper alkaline fluids, direct proxy of current serpentinization (Abrajano *et al.*, 1988; Barnes *et al.*, 1967; Deville and Prinzhofer, 2016; Neal and Stanger, 1983), have to be mapped. Conversely, in intracratonic contexts, a relation between the presence of SCDs and the presence of H_2 has been made and the study of SCDs is very useful in such contexts, although obviously, the presence of SCD is neither necessary nor sufficient, to confirm, or invalidate, an H_2 accumulation.

3 Fieldwork: sampling and measurements

3.1 Gas

For all the aforementioned source types of H_2 emissions, different sampling protocols have been used in the past years based on the experience of other gas emanations. Before collecting the gas, the first step is to channel the flux in an adapted way to prevent any additional air contamination. Then two main ways of sampling exist depending on the analyses of interest and the gas content.

3.1.1 Sampling

3.1.1.1 Channelizing the gas flux

Based on literature and field trip experiences, Figure 9 presents various ways to efficiently channel fluxes depending on their source types.

For the free gas vents (Fig. 9a) or bubbling water (Fig. 9b), the protocol detailed in Pasquet *et al.* (2021) can be used. It consists in placing a funnel upside down just above the gas flow. Our funnel is connected to a silicon tube that is resistive regarding elevated temperatures around 100 °C. By putting the extremity of the tube in a water container and observing the formation of bubbles, we ensure that the gas flux circulates in the whole tube and that no contamination of atmospheric air comes by the exit of the tube. We recommend waiting several minutes for gas bubbling in the container to expel any ambient air remaining in the tube and to flush the line with the gas of interest. In the case of bubbling water sources, the protocol is the same, except that the funnel should be placed below the water surface to prevent air contamination.

For boreholes (Fig. 9c), the channelizing is already done by the casing itself. As described in Guélard *et al.* (2017), a plugged drill hole header prevents any air contamination and allows the accumulation of the free gas phase or the water pressure depending on the artesian pressure inside the drill hole. In the case of an artesian well, connecting the borehole plug valve to a semi-closed container is necessary to favor the gas exsolving.

Contrary to other source types, soil gas (Fig. 9d) is much more difficult to channelize since the involved fluxes are discontinuous and much weaker. We can note that no consensus yet exists on the right way to sample

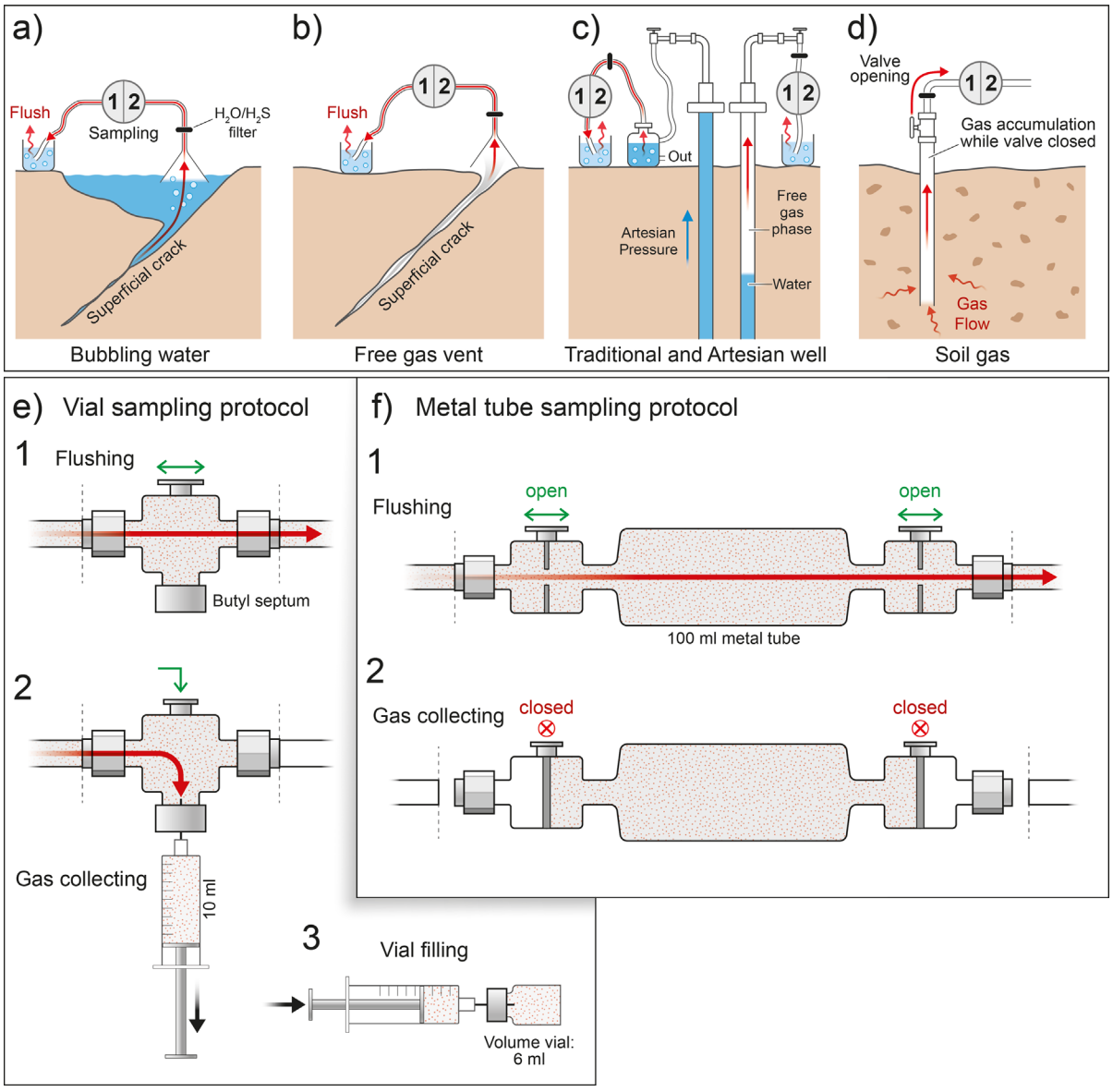

Fig. 9. Simplified schemes of H_2 gas sampling after channelizing the flux in four different contexts: (a) bubbling water, (b) free gas vent, (c) a well, and (d) soil gas. (e) Sampling into a vial and (f) sampling into an aliquot.

it. A one-meter-deep hole can be drilled in the soil at first. To limit H_2 generation artifacts related to the drilling, percussion rather than rotation should be privileged (Lefeuvre *et al.*, 2021) but from our experience, the results are often the same. Afterward, a tube equipped with several holes at the bottom is pulled down in the drilling hole, channelizing the gas to the top of the tube. By closing the valve at the top of the tube, the soil gas moving upward starts to accumulate and can be sampled after various times of accumulation depending on the flux involved (hours to days).

3.1.1.2 Sampling: vials vs. aliquots

The first method presented in Figure 9e shows gas sampling into vials usually applied for major gas analyses. The technique consists of connecting a three-way valve on the tubing to channel the gas flux. One of the three ways is equipped with a butyl septum and allows gas to accumulate after the flushing. Stinging the septum of the vial already under vacuum with a syringe, the pressurized gas is then collected. Although the container septum should be completely gas-tight, we suggest slightly overpressurizing the glass container to ensure that the gas leak is oriented outward in case of minor septum breakdown during transportation and thus preserves the quality of the sample. Usually, we roughly overpressurize by a factor of 1/3. To go further, varnish should also be added to cover septums where they have been stung in the case of prolonged sample storage. The use of vials is fast and economical and thus appears very appropriate when a lot of samples are collected. However, as described earlier, the method involves several sources of possible contamination during sampling,

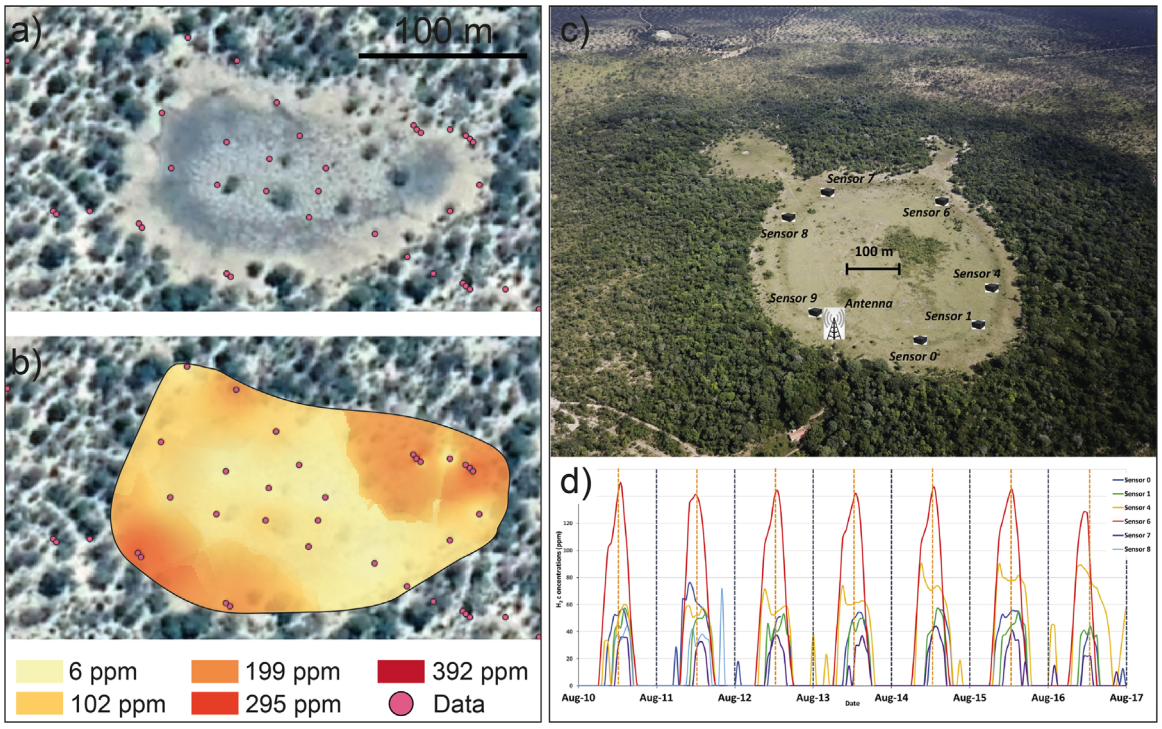

Fig. 10. (a) Satellite image of an SCD in Namibia and (b) the associated heat map of H_2 concentration in soil gas after extrapolating from punctual BIOGAS GA5000 measurements. (c) Long-term monitoring of an SCD in Brazil (Prinzhofer *et al.*, 2019) and (d) Intensity of H_2 plotted against time that shows H_2 periodic pulses. See Appendix B for coordinates.

transportation, and storage: among others, the use of a syringe with a needle that is in contact with atmospheric air and/or the uncertainty concerning the air tightness of the septum are major sources of possible additional sample contamination.

For higher-quality sampling, another standard technique detailed in Figure 9f is used. This method consists of connecting the gas container, called an aliquot, directly to the tubing to drive the gas flux. The aliquot is equipped with close/open valves at each extremity, allowing the sampling system to be separated from the channelizing tubing. While the flux is high enough, we recommend collecting the gas by closing the valves after several minutes of flushing, to ensure the sampling purity. Such a technique is very efficient for sampling but implies at least extras in terms of logistics and therefore only a few samples were collected. However, this method is recognized as very efficient while working on very low-concentrated gas, in the noble gas field, for example.

3.1.2 Gas measurements

3.1.2.1 Punctual acquisitions

Measurements. First *in situ* measurements of H_2 were related to safety issue and earthquake prediction. It has been done for instance in the USA along the San Andreas Fault (Sato *et al.*, 1986) or in Russia in the early 2000s (Firstov and Shirokov, 2005). At this time, a geophysical H_2 detector was designed, based on a change in the capacitance of the metal–insulator–semiconductor electronic transition under the influence of hydrogen in the soil. The instrument was used during several field campaigns in the following years for punctual acquisitions (Larin *et al.*, 2015; Zgonnik *et al.*, 2015), before being progressively abandoned in aid of geochemical detectors.

Over the last years, the portable instruments GA2000 and then GA5000 or BIOGAS5000 from *Geotech*® became the norm (Fig. 10a) (Frery *et al.*, 2021; Lefeuvre *et al.*, 2021; Leila *et al.*, 2021; Lévy *et al.*, 2023; Moretti *et al.*, 2022; Pasquet *et al.*, 2021; Prinzhofer *et al.*, 2019). However, sampling the gas within the first meters of soil could be challenging and frustrating due to the very large air content in the close-to-surface soil, usually more than 95 vol.% with, depending on the cases, few vol.% of CH_4 or CO_2. These instruments are equipped with H_2-sensitive electrochemical cells able to quantify H_2 from 0 to 1000 ppmv with a precision down to the ppmv and thus revealed as very efficient tools. In addition, they also detect O_2, CO_2, CH_4, and optionally CO and H_2S. The analyzer does not measure directly the N_2 but gives a balance value usually interpreted as the N_2. The number of detected gases could be customized when purchasing the sensors. One limitation of the GA instruments resides in the H_2 detection threshold of 1000 ppmv that prevents an H_2 quantification while seeps are H_2-rich. To get through this limitation, the use of the Variotec 460 Tracergas is starting. This instrument, originally designed to detect leaks of H_2 in industrial infrastructures and construction sites, is now used for H_2

exploration. Its main advantage is its ability to cover all ranges of H_2 concentrations from 0 to 100 vol.%. It is composed of two different detectors, measuring H_2 from 0 to 10000 ppmv with a precision down to the ppmv and the second from 0.1 to 100 vol.% with a precision of 0.1 vol.%. As the Variotec instrument only detects H_2, combining its use with the use of the GA5000 instrument appears as efficient to evaluate the repeatability of the measure as well as to obtain the whole gas composition during field acquisitions. These instruments are not the only ones and other portable gas analyzers exist on the market such as the Optimax (MRU instrument) which is rather similar that the GA.

Limitations. Several limitations should be pointed out concerning such punctual measurements. Concerning the utilization of these apparatuses, pumping is necessary to transport the gas to the detector. The pumped volume is rather high, up to 500 mL/min, and could source contamination from atmospheric air pumping if the contact between the tube and the walls of the void is weak during soil gas measurement. To avoid this bias, it is important to have the diameter of the drillbit close to the tube diameter. We also notice that this volume is decreasing all over the day in parallel to the decrease of the battery charge. The pumped volume cannot be considered constant during the whole field campaign. On the other hand, this pumping power actually corresponds to a very small volume of soil around the stem. Given the average permeability of soil at this depth, only 2 cm around the tube is drained (Moretti *et al.*, 2021a). These analyses therefore only study a very small part of the soil and if we do not pump, it is even worse. The quality of the H_2 analysis is also a matter of debate during soil gas measurements since, as already noted, the drilling that precludes the measure could artificially generate H_2 and create artifacts (Lefeuvre *et al.*, 2022). However, the large amount of "zero values" collected during all the field trip campaigns suggests that such artifact effects during drilling might be limited, if present. Supplementary material provides an extensive dataset of measurements, the "zero values" obtained over various acquisition campaigns in Namibia, Australia, Bolivia, Ethiopia, and the Republic of Djibouti clearly show that the H_2 generation when drilling a few tens of centimeters in the soil is rare. From our experience, it happens when the drill bit is getting very hot and, in that case, the H_2 content is proportional to the duration of the perforation. The H_2 signal evolution during the 2 min of the measurement is rather different and easily detectable. Usually, with a GA5000, the maximum H_2 is reached between 30 s and 40 s.

Representativeness. Concerning the representativeness of one measurement on an H_2 seeping system, studies demonstrated a strong variability in space and time of H_2 fluxes, particularly in the case of soil gas (Moretti *et al.*, 2021b; Prinzhofer *et al.*, 2018; Zgonnik *et al.*, 2015). As such, getting a "zero value" should not be considered proof of a non-emitting H_2 system, as well as getting one high H_2 value should not be considered evidence of an active H_2 system. The efficiency of such portable instruments lies in the ease to multiplicate the number of analyses in a short lapse of time and thus get free from the aforementioned bias. Statistical work based on several hundreds of measurements allows us to draw global trends (Moretti *et al.*, 2022), so we suggest doing at least a few tens of measurements in each studied SCD. On the other hand, in the areas where systematic soil gas measurements have been done in various SCDs, it seems that their behavior is very similar (Brazil, Moretti *et al.*, 2021a; Prinzhofer *et al.*, 2019; Namibia, Moretti *et al.*, 2022; Australia, Frery *et al.*, 2021). The strategy could be to select one of them after a few random measurements and then do a hundred measurements in a given one at different times of the day. We suggest also extending the measurements out of the area without vegetation. In case of a fault leaking, the H_2 content in the soil are depending on the distance to the fault and so cross-sections perpendicular to the fault scarce (even if it is not visible) should be done (Lefeuvre *et al.*, 2022).

3.1.2.2 Long-term monitoring

Long-term monitoring, essentially implemented for the study of soil gas H_2, allows us to better define the space and time variability described above. The principle is similar to *in situ* soil gas measurements. An H_2 probe is buried at a shallow depth of about 1 m. Automatic measurement is performed regularly over long periods. So far, the main example of such monitoring is the study conducted on H_2-emitting SCDs in Brazil (Fig. 10b) (Moretti *et al.*, 2021a; Prinzhofer *et al.*, 2019). There, two structures were monitored for 6–8 months by the means of 44 and 51 PARHyS detectors developed by Engie programmed to get one measurement per hour (Rosanne, 2020). Cyclic pulses were observed in H_2 levels, with a maximum during the days and a minimum during the nights. The origin of this periodic signal remains a matter of debate but it could come from atmospheric pressure variations (Cathles and Prinzhofer, 2020) or cyclic pulses in-depth (Myagkiy *et al.*, 2020a,b). The earth's tide, on the opposite, happened to be neglectable and unable to explain the single daily maximum (Simon *et al.*, 2020).

In addition to this soil breathing with a 24 h period, the long-term monitoring showed large pulses, that usually saturated the regular sensors for 2 days and are unpredictable on our current knowledge. They are rare, when 10 sensors were installed for 2 months, only one large peak has been recorded (Prinzhofer *et al.*, 2019). Among the hundred sensors, which were at a distance of about 80 m, one recorded almost one large pulse per week (Moretti *et al.*, 2021a). The pump power of the PARHyS has been adjusted to that of the GA5000 for comparisons and therefore the volume of soil, which is analyzed during the 2 min long measure, is small and corresponds to a distance of drainage of about 2 cm. The lack of correlation between the signals measured from the various sensors seems to indicate that the H_2 pulses measured with this monitoring correspond to independent events that affect only a small zone. It is therefore more representative to use tens of sensors. The previous authors concluded that there is no way to deduce an average behavior of a structure from just a couple of measurements.

Concerning the tools available for these permanent measurements one may note that various laboratories are

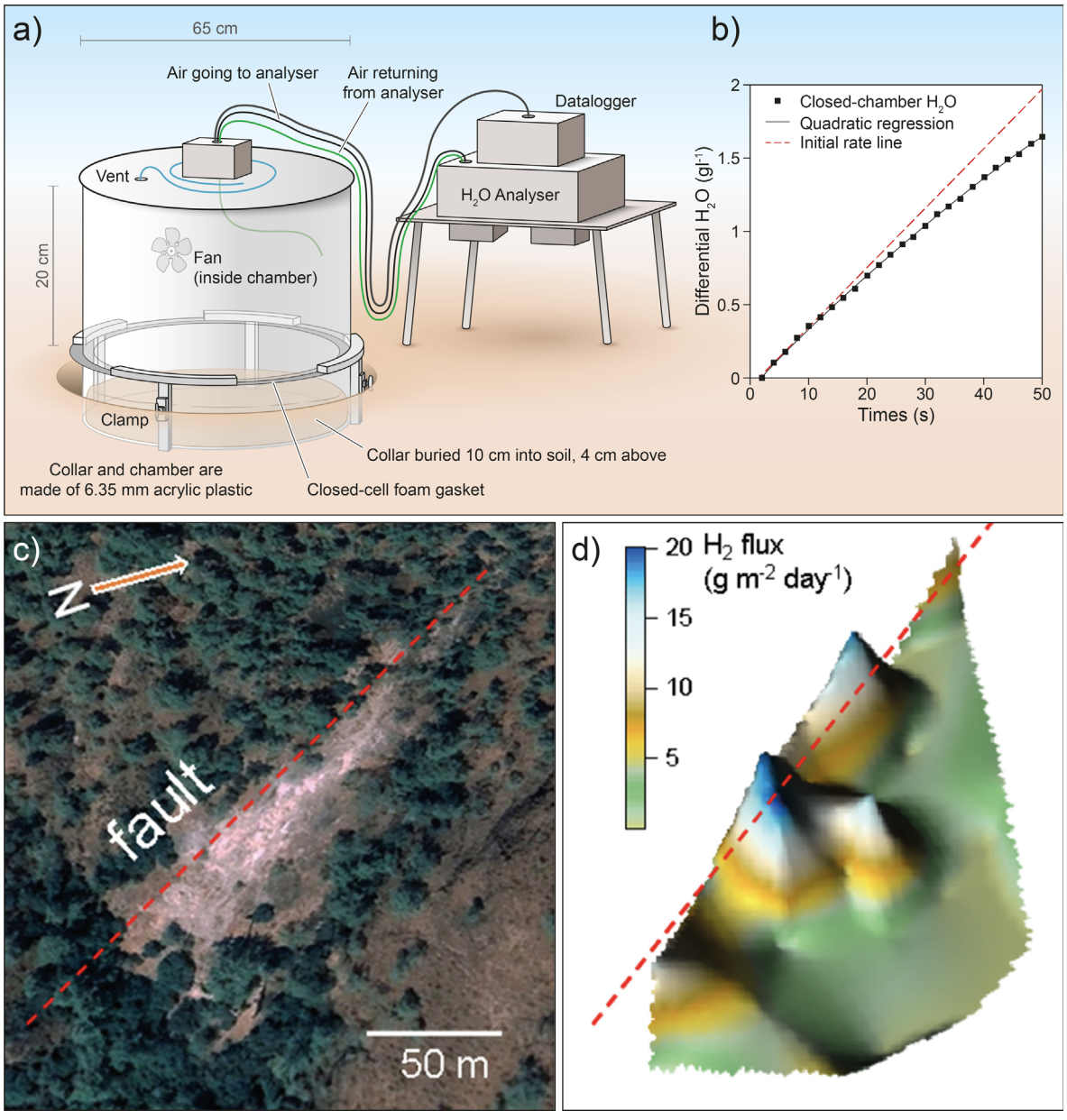

Fig. 11. Flux sampling. (a) Closed chamber apparatus scheme designed for measuring CO_2 in soil gas (Rochette *et al.*, 1997). (b) Evolution of H_2O concentration in a closed chamber through time, fitted with a non-linear equation (Wagner *et al.*, 1997). (c, d) Gas fluxes map acquired on the Chimaera seep with the associated satellite image (Etiope, 2023). See Appendix B for coordinates.

currently working on new ones. The companies *45-8 Energy* and *Solexperts* launched SurfMoG H_2 in February 2023 for undergoing H_2 monitoring. But, on-site comparisons are not yet available. With these techniques, we can measure repetitive concentrations to try to compute a recharge flow within the soils.

3.1.2.3 Gas fluxes estimates

Once the concentrations are measured, evaluating the fluxes may help to quantify the emitted H_2 volumes, since 100 vol.% of H_2 in a very low flux seep could be less interesting than 1 vol.% of H_2 in a very high flux seep. In the case of H_2 emissions from free gas vents, bubbling water, or boreholes, estimating the fluxes should be easy as they are high enough to be channelized and measured with a flowmeter without air contamination. On the contrary, H_2 fluxes from soil gas are low, and quantifying them cannot be done using a simple flowmeter tool.

Over the years, efficient tools have been developed to study soil gas fluxes such as closed chambers (Figs. 11a and 11b), which progressively adapted to the study of H_2. The principle consists in measuring the evolution through time of a gas of interest in a closed chamber settled onto the soil ground. Since the exact volume and the footprint

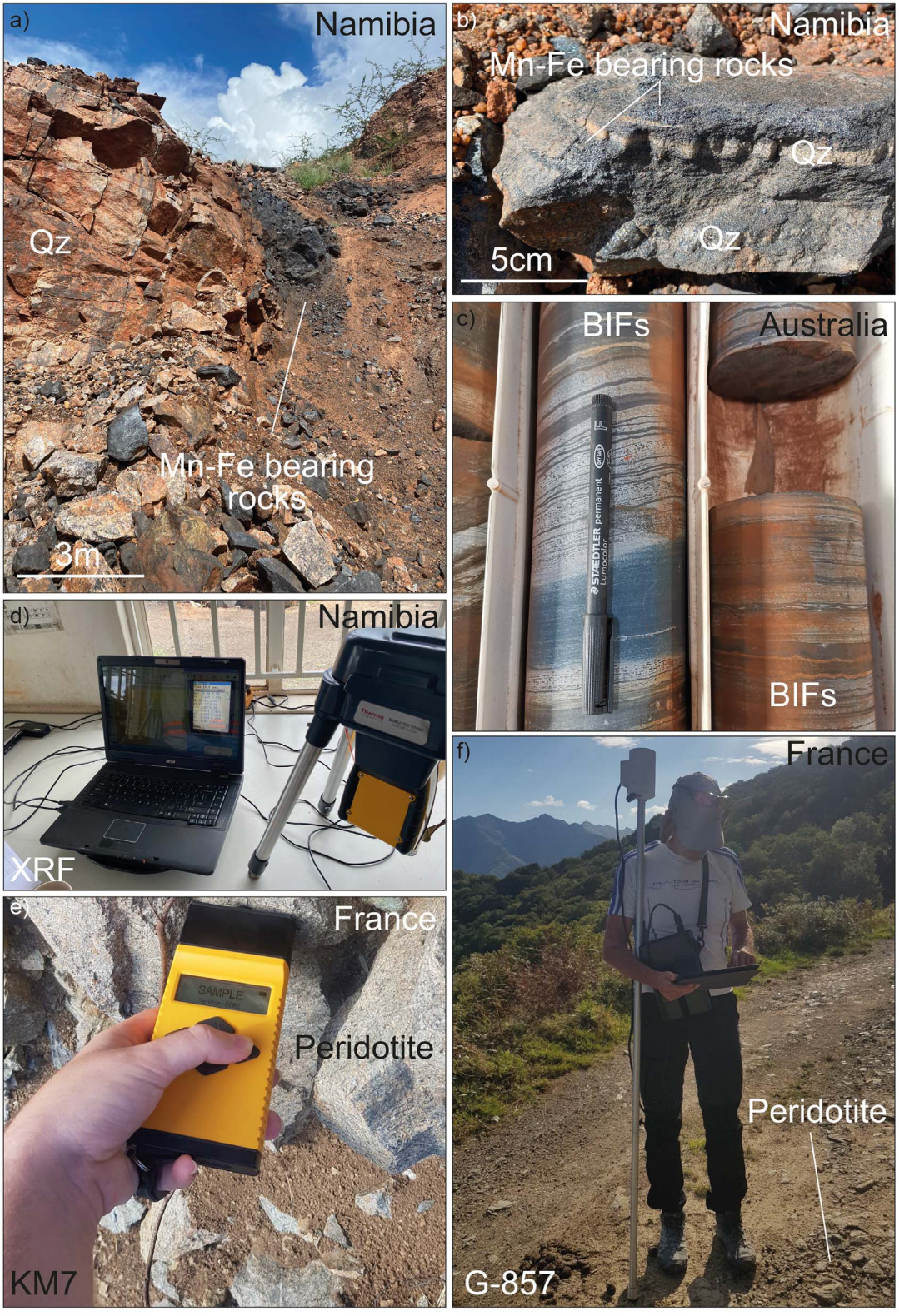

Fig. 12. Images showing different outcrops, samples, and various *in situ* analyses. (a, b) Mn-Fe bearing rocks in Namibia. (c) BIF core from Australia. (d) Portable XRF instrument for *in situ* major element analysis. (e, f) Kappameters KM7 and G-857 for magnetic susceptibility measurements. See Appendix B for coordinates.

of the chamber are known, a correlation between the time and the gas concentration in the chamber can be established following linear or exponential laws, giving access to gas fluxes, for instance in $mol.m^{-2}.d^{-1}$ (Wagner *et al.*, 1997). Recently, the first study dedicated to evaluating H_2 flux thanks to closed chambers was on Chimaera-free gas vents (Etiope, 2023). Within the closed chamber, 30 cm in diameter, a concentration measurement was realized every minute. A flux map of the area was built, providing results with natural H_2 fluxes up to 5000 $kg.km^{-2}.d^{-1}$ (Fig. 11c). One may note that the chamber is not always the right choice because it can affect the flow or even stop it when it is mainly diffusive, which can result in artificial low values.

Nevertheless, we must keep in mind that what we measure with the closed chamber or permanent sensors is just some leakage. They are reassuring about the existence of an active H_2 system but say nothing about the subsurface reserves and even about the deep flow. Spending too much time to perfectly measure these H_2 soil gas contents will not, in our opinion, decrease the uncertainties inherent to the exploration phase.

3.2 Rocks

Sampling rock is essential for understanding the various processes that can generate H_2. This implies that sampling needs to be done in accordance with standard practice in the mining industry. In that sense, cross-sections combined with structural measurements must be performed, for example, to understand the global geological framework of the rocks sampled and/or to estimate the volume of an interesting lithology. The pressure-temperature evolution changes also the characteristic of the rock and may influence the content of Fe^{2+}. This is the case in Namibia where magnetite-bearing rocks are mainly found in highly metamorphic units in the Damara Belt (Figs. 12a and 12b). Further, in the case of H_2 from water/rock interactions, many studies showed a very large heterogeneity of *e.g.* iron content in rocks at all scales ranging from a few millimeters to several kilometers. It is, therefore, necessary to take several samples at different places to reflect heterogeneities. In addition to the outcrops, some countries (*e.g.*, Australia and the USA) provide free access to their core libraries for both researchers and operators, particularly for the cores from previous drilling programs. When well data are available, cores or cuttings are ideal for obtaining a complete description of the generating interval, like the description of the cuttings in the Asal Rift and the identification of an H_2 system (Pasquet *et al.*, 2023). They also avoid the effects of near-surface weathering, which can affect the Fe^{2+}/Fe^{3+} ratio (Fig. 12c).

Depending on the H_2_GR studied, several methods and approaches may be used in the field for rock examinations. X-Ray Fluorescence (XRF) is one of them (Fig. 12d). This method is fast, reliable, and non-destructive and provides access to major element concentrations in the rock. Further, magnetic susceptibility could also be a fast field proxy to determine the state of alteration/serpentinization. The magnetic susceptibility of a rock is controlled by the type and amount of magnetic minerals in its paragenesis (Martín-Hernández *et al.*, 2004), and the main carrier of this signal is the magnetite due to its ferromagnetic behavior. Field measurements are quite simple and fast when the H_2_GR is outcropping. Kappameters allow to acquire the magnetic susceptibility, such as the portable KM7 that only requires a small plane interface to perform the measurement (Fig. 12e). To avoid the impact of the weathering, these measurements have to be performed on fresh outcrops. In addition, measurements of the magnetic field could be done in the same type of rocks. This can be performed using a G-857 Memory-Mag Proton Precession Magnetometer (Fig. 12f). The magnetic field measured on the surface corresponds to the interaction between the external core's magnetic field and the magnetic behavior of the minerals.

3.3 Workflow for the fieldwork

The workflow developed for *in situ* gas measurements is given Figure 13. After punctual analyses, the locations of H_2-rich locations can allow us to perform long-term monitoring and gas flux assessment. In addition, the rocks associated with the gas can be analyzed *in situ* by different techniques (*e.g.*, XRF, magnetism). The sampling of H_2-rich gas and rocks is finally done to make laboratory analyses.

4 Post-fieldwork: laboratory analyses

The rocks and gas samples collected during fieldwork must be analyzed in the laboratory to conduct further chemical and petrological measurements since they both hold complementary clues to understanding the "whole" H_2 system. Rocks carry evidence of the mechanisms leading to H_2 generation at depth, while gases provide insights into physicochemical parameters and the source. Numerous analytical tools are available for the full characterization of rock and gas samples. This section aims to present those analytical techniques that appear essential for the study of H_2-related seepages and H_2-generating rocks.

4.1 Gas characterization

4.1.1 Bulk gas chemical quantification

Following the semi-quantitative and limited measurements during the fieldwork, the precise characterization of the gas samples in the laboratory should begin with the study of the bulk gas chemical composition. Here, quantifying H_2 levels is of prime interest because (i) it validates or invalidates the discovery of H_2 seepages and (ii) provides information about the total amount of H_2 emitted, which could be used to estimate the leakage coming from the depth. Several gaseous species are commonly found in association with H_2-related seepages such as O_2, N_2, He, Ar, light HC, or CO_2. Their respective abundances in the

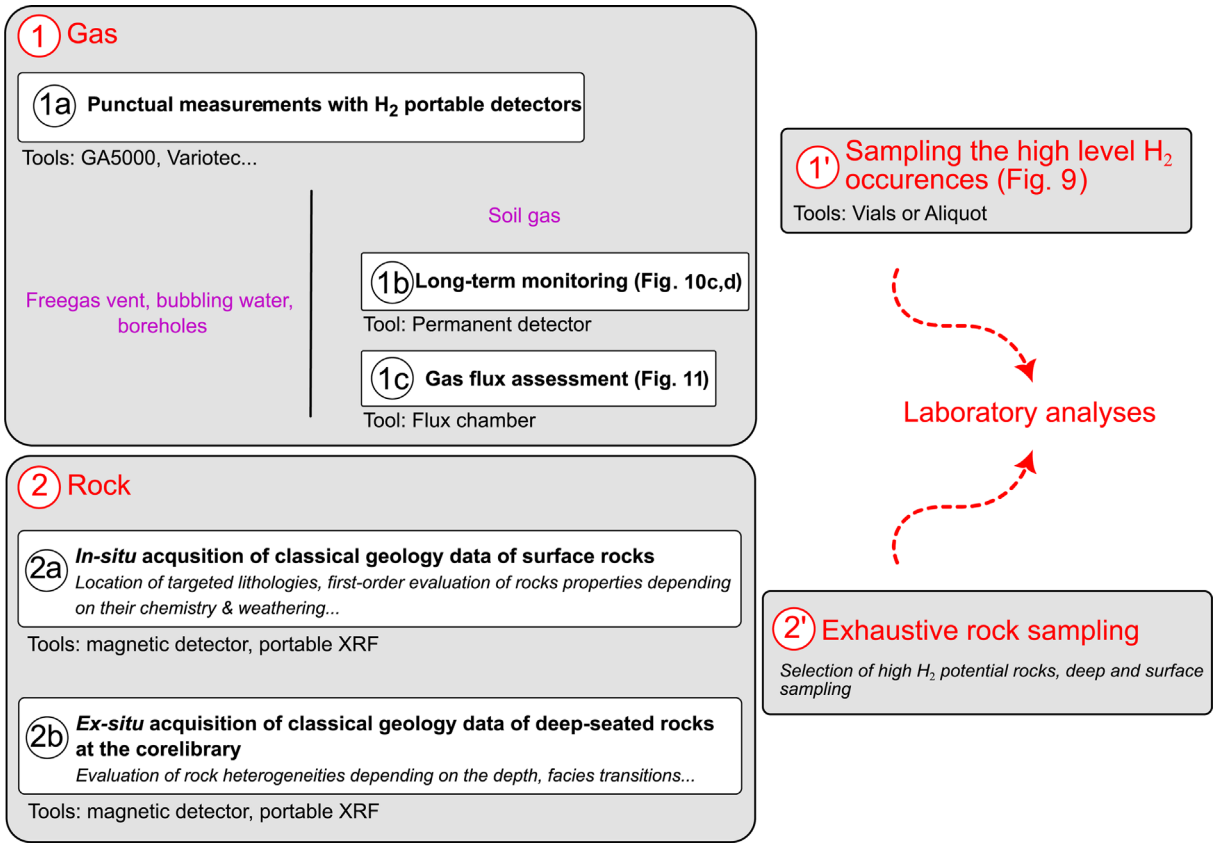

Fig. 13. Fieldwork proposed workflow. *In situ* measurements and sampling strategy for gases and rocks.

gas mixture hold clues to understanding the dynamic of the H_2 system at depth, which are discussed. For instance, high levels of crustal He in the bulk gas could be seen as a marker of radiolysis because the radioactive decay produces He.

Among the variety of tools available to determine the bulk gas composition, Gas Chromatography (GC) is the most used for H_2 exploration. GC devices are often equipped with a Thermal Conductivity Detector (TCD) that provides a good compromise between a wide range of species detection and quantification accuracy, especially for inorganic compounds (Guélard *et al.*, 2017; Lefeuvre *et al.*, 2021; Zgonnik *et al.*, 2015). For the specific purpose of organic gases quantification associated with H_2, such as light hydrocarbons, an additional Flame Ionization Detector (FID) is used offering a higher degree of precision than a TCD (Prinzhofer *et al.*, 2018; Sherwood Lollar *et al.*, 2006).

4.1.2 Isotopic composition

In nature, the atoms of the same element can have different masses, named isotopes. The isotopic composition of a gas is usually measured by Isotopic Ratio Mass Spectrometer (IRMS), and in some cases directly connected to a GC. After passing through the GC, the gas is ionized. Ions are then separated depending on their mass/charge ratio which allows us to measure the isotopic ratios.

The isotopic composition reflects the fractionation mechanisms occurring during geological processes. Two types of isotope fractionation exist: (i) equilibrium fractionation and (ii) kinetic fractionation. In the first case, the isotopes fractionate following the thermodynamic law that depends mainly on temperature evolution. For example, while two chemical species carry the same element, like H_2 and H_2O, the H isotopic abundance of both species is known to isotopically equilibrate through the reaction (2) as a function of a thermodynamical law dependent on temperature (Horibe and Craig, 1995). In the second case, the isotopes fractionate depending on their masses. The higher the relative difference of mass between isotopes, the higher will be the fractionation.

$$H_2O + HD = HDO + H_2. \quad (2)$$

For H_2-related seepages, the isotopic composition of H_2, CH_4, CO_2, N_2, and He are usually measured (if present), since the isotopic signatures of these gases give access to physicochemical parameters related to H_2 origin, trapping, and migration. For instance, as previously mentioned, He enriched in ^{4}He is known to originate from radiolysis (Ballentine and Burnard, 2002). Thus, a ^{4}He-rich seepage infers crustal H_2 formed via radiolysis.

In the discussion, the δ, ε, and R/Ra notations are used. They are presented with the example of H isotopes:

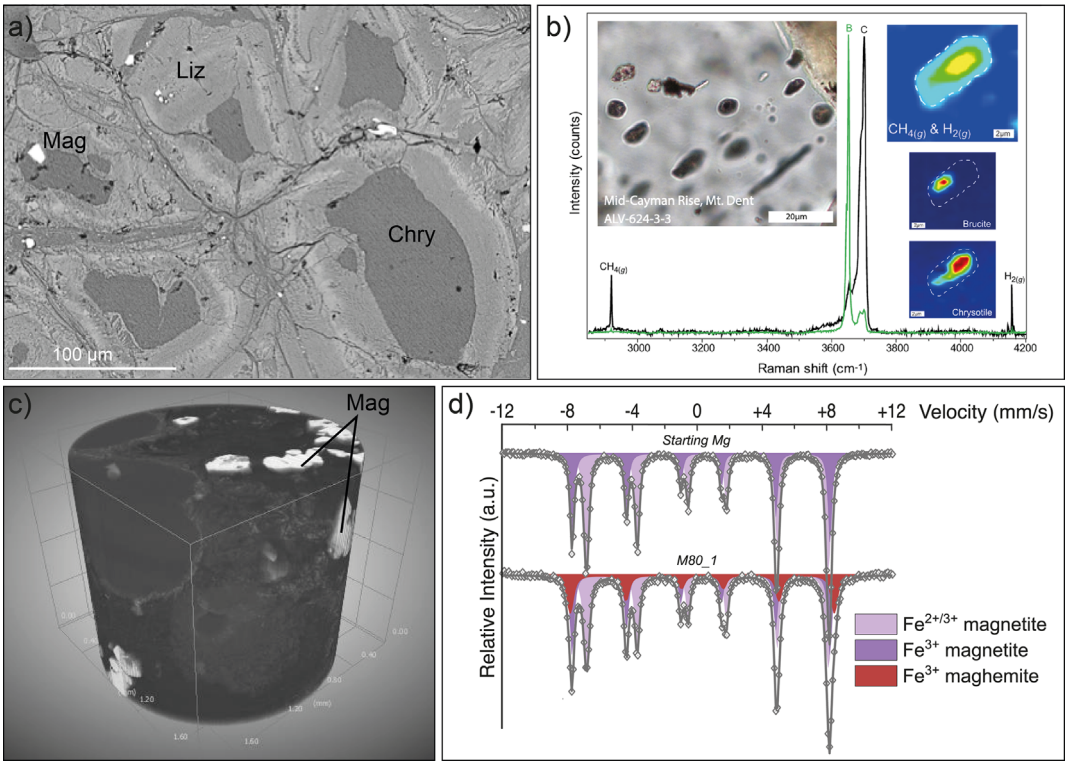

Fig. 14. Techniques used to characterize the H_2 potential of rock. Data from (a) scanning electron microscopy of a serpentininte (modified from Lévy *et al.*, 2022), (b) Raman microspectroscopy on H_2-rich fluid inclusions (modified from Klein *et al.*, 2019), (c) X-ray microtomography (acquired on a Zeiss Radia Versa 510, DMEX), and (d) Mössbauer spectroscopy of a BIF (modified from Geymond *et al.*, 2023). Chry: chrysotile, Liz: lizardite, Mag: magnetite.

$$\delta D = ((D/H)_{sample}/(D/H)_{standard} - 1) \times 1000. \quad (3)$$

$$\varepsilon = 1000 \times \ln((D/H)_{sample}/(D/H)_{standard}). \quad (4)$$

$$R/Ra = ({}^3He/{}^4He)_{sample}/({}^3He/{}^4He)_{atmospheric}. \quad (5)$$

4.2 Petrographic characterization

The analytical tools for petrography can be broadly divided into two categories: (i) tools that provide quantitative information on samples (*e.g.*, amount of Fe, size of minerals) and (ii) tools dedicated to observe samples at various scales. In the specific context of H_2 exploration and considering that the content of specific elements (Fe, U, K, Th, or Organic matter) is key to assess the H_2-generating potential of rocks, we believe that the quantitative tools are more important. From a fundamental point of view, however, observing the paragenesis is important to improve the knowledge about H_2 dynamics (*e.g.*, which mineral is highly reactive or not, at which temperature). All the tools and their characteristics are listed in Appendix C.

4.2.1 Bulk quantification tools

When investigating the H_2 potential of lithologies related to water-rock interactions, ICP (Inductively Coupled Plasma – Mass Spectrometry or Optical Emission Spectroscopy) and XRF (X-Ray Fluorescence spectrometry) are the techniques to get access to Fe, U, Th, and K as well as other major and trace element concentrations in the bulk sample. Their operating principle does not allow us to know the redox state of the elements. In the case of Fe-oxidation-related H_2 generation, the redox state of the element is meaningful information because it determines whether a rock is still able to produce H_2 currently. Although other techniques exist for this purpose, such as titration in solution associated with ICPs, ^{57}Fe Mössbauer spectroscopy should be privileged to obtain Fe-speciation in the bulk rock sample. Using this method, the redox state is obtained in each mineral family constitutive of the bulk rock sample. It must be said that all information provided at the bulk rock sample scale can also be collected at a mineral scale, using other techniques that are not described here.

X-Ray Diffraction (XRD) is commonly used to evaluate the mineralogy of the bulk rock sample and thus to determine which phase carries the element of interest (*i.e.*, Fe, U, Th, or K). Thanks to quantification algorithms such as the Rietveld method, the proportion of each phase in the mineral assemblage can be assessed.

When investigating the H_2 potential of organic matter-rich rocks, evaluating the Total Organic Content (TOC) and the paleo-maturation is essential. The Rock-Eval pyrolyzer, used for decades by O&G companies (Behar *et al.*, 2001; Espitalie *et al.*, 1980), gives this information.

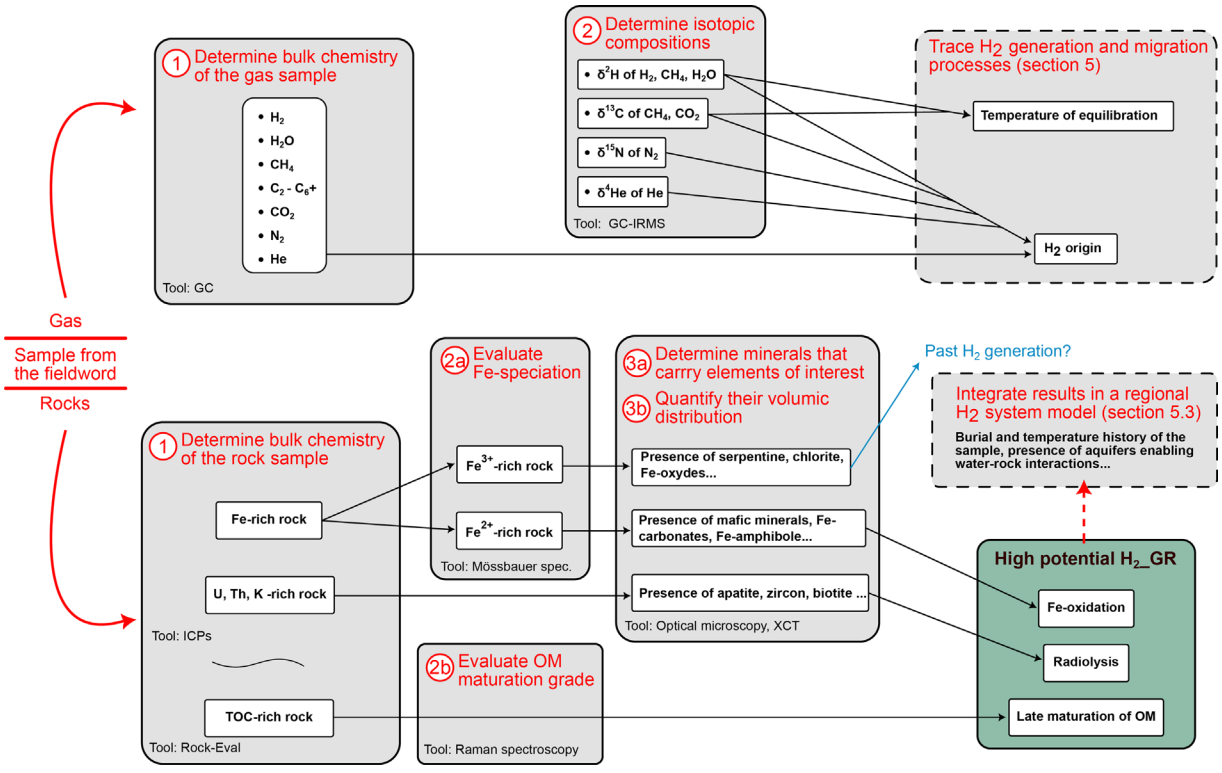

Fig. 15. The workflow developed for laboratory-based gas and rock analyses of the potential H_2_GR.

Additional paleotemperature markers could be used to cross-check the pyrolyzer's results, such as the Vitrinite Reflectance or Raman data. For the coal, the rank may be also quantified, affecting the kinetics of pyrolysis and the H_2 generation potential (Yan *et al.*, 2020; Zhang *et al.*, 2020).

4.2.2 Observation tools

While trying to understand the generation of H_2, observing the samples to complete bulk rock chemistry and mineralogy quantitative analyses becomes mandatory (Fig. 14). For instance, if we consider a Fe-rich rock that is known to source H_2, and that carries two different Fe-rich minerals, the only way to determine which mineral sources H_2 is to observe them at the microscopic scale, and thus collect information about their respective stabilities in the mineralogical assemblage. Two different types of observation tools exist: (i) optical and (ii) electron microscopy. They essentially differ by the nature of the particle (photon or electron) interacting with the sample and the size of the feature they are able to image. Optical microscopy allows us to work at a resolution reaching down to a few microns. At such resolution, alteration rings surrounding Fe^{2+}-minerals being altered, H_2-bearing fluid inclusions, as well as radioactive decay halo within biotite, are interesting features to observe (Fig. 2). Electron microscopies such as Scanning Electron Microscopy (SEM) or Transmission Electron Microscopy (TEM) should be used to reach a higher resolution, down to the nanometer. Combining electron microscopy with *in situ* quantitative techniques such as Electro Probe Micro-Analyzer (EPMA) enables us to know precisely the chemistry of minerals of interest and draw conclusions about the processes sustaining H_2 generation.

4.2.3 Representativeness of data

The representativeness of the previously described analyses and observations could be challenged while trying to conclude, especially when the study aims to characterize the potential of a geological formation as H_2_GR.

At the sample scale first, it must be kept in mind that imaging techniques provide 2D information, such as the mineral abundances in the thin section, that are not always representative of the 3D equivalent volume. Only X-Ray Microtomography (XCT) can tackle this limitation since this technique allows us to image and quantify minerals distribution in cm^3–m^3 rock plugs. Otherwise, bulk rock analyses should be privileged to favor the representativeness of the results.

At the geological formation scale then, it is reasonable to imagine that natural rocks can present heterogeneities in composition, or different degrees of alteration in the case of water-rock interactions, along the stratigraphic column. Thus, it appears fundamental to study multiple samples and cross-reference the acquired information to obtain a realistic characterization of the H_2_GRs.

4.2.4 Workflow for H_2-generating rocks

The workflow developed for laboratory-based gas and rock analysis is given in Figure 15. We have selected what we believe are the most efficient and complementary tools to

quickly characterize the H_2 potential of an H_2_GR whether it is related to iron oxidation reactions (H_2_GR1 and H_2_GR2), radiolysis (H_2_GR3) or late organic matter maturation (H_2_GR4). To ensure the representativeness of the H_2 potential assessment of the generating rock, one should consider performing this workflow on multiple samples coming from different depths within the studied rock formation.

- First, an ICP analysis should be done to determine the total bulk concentrations of elements of interest such as Fe, U, Th, or K. Rocks without one of these compounds in significant amounts should be disregarded as a potential H_2_GR.
- In case of suspected overmature TOC-rich source rock, a Rock-Eval analysis should allow to distinguish organic-rich rocks H_2_GR4, the maturation should also be quantified. It could be done directly from the pyrolyzer data if the characteristics of the immature source rock are known but additional values such as vitrinite reflectance or other paleothermometers allow additional quantification.
- Second, ^{57}Fe Mössbauer spectroscopy should be performed on iron-rich rocks to determine the speciation of Fe. Fe^{2+}-rich rocks should be considered as high H_2 potential generating rocks regarding redox processes while Fe^{3+}-rich rocks should not be considered as potential generating rocks for future H_2 production, although they could have produced H_2 in the past.
- Third, identification of the minerals that carry Fe^{2+}, U, Th, or K should be performed on thin sections using optical and electron microscopy. The identification of Fe-bearing minerals should help to assess the H_2 potential of the rock, depending on the proper reactivity of each mineral during water-rock interaction.
- Finally, XCT should be done on core samples to extrapolate at a larger scale the quantifications and observations made at low scale, and thus estimate the true potential to source H_2 normalized to its volume. It must be noted that XCT is essential to efficiently evaluate the true potential of the H_2_GRs as it allows to consider of mineralogical heterogeneities at a micrometric scale. It is mandatory to know the mineral assemblage of the studied rock to correctly identify the Fe or U, Th, K-bearing phase in the studied XCT volume.

5 Discussion

5.1 Significance of measuring gas composition

5.1.1 Bulk data

The major gases commonly associated with H_2 are CH_4 and N_2. The H_2-CH_4-N_2 ternary diagram presented in Figure 16 is therefore usually used to plot the gas data. Attempts to classify the different ophiolitic sources have been made (Vacquand *et al.*, 2018). Regarding the gas data that contain H_2, CH_4, and N_2 as major gases, we observe the N_2-CH_4 trend and the H_2-CH_4 trend. However, it remains difficult to differentiate a source type based on the H_2-CH_4-N_2 ternary diagram. The most H_2-rich gas is from the well of Bourakebougou in Mali (Prinzhofer *et al.*, 2018).

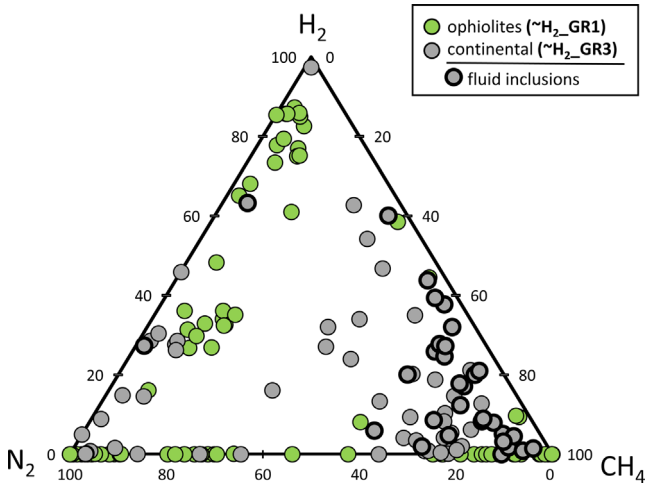

Fig. 16. H_2-CH_4-N_2 ternary diagram showing H_2-rich gas samples collected from ophiolites and continental crust (Coveney *et al.*, 1987; Etiope *et al.*, 2017; Guélard *et al.*, 2017; Lévy *et al.*, 2023; Nivin 2019; Potter *et al.*, 2013; Randazzo *et al.*, 2021; Salvi and Williams-Jones, 1997; Sherwood Lollar *et al.*, 2006; Vacquand *et al.*, 2018).

This diagram does not include other gases and one has to check if H_2, CH_4, and N_2 are indeed the major gases to best interpret it. For example, CO_2-rich sample data usually plot in the N_2-CH_4 trend.

The data on hydrocarbons C2-C6+ are important because their presence can give indications about a source related to a petroleum system for example. But if we want more insights into the physicochemical parameters related to the gas, we need to use the isotopes as done in the next section.

5.1.2 Isotopic data

The isotopic data can be used as geothermometers when possible and as tracers of the different geological sources. A compilation of available isotopic data in the literature from ophiolites (~H_2_GR1), and intracontinental areas (~H_2_GR3) is given in Figure 17.

When compiling the H isotopic data (Fig. 17a), we observe that the δD (3) of H_2 measured on ophiolites are lower than −585‰. Most of the data of the H_2 continental measurements have also a δD lower than −600‰. However, some data from Sherwood *et al.* (1988) are up to −138‰ and desorption data from Truche *et al.* (2018) also show high δD. The δD of H_2 alone is not an efficient tool to discriminate one source from another. However, it can be combined with the assumed/measured δD of H_2O, often used as a geothermometer to evaluate the last temperature of equilibration of H isotopes. However, the δD of H_2O is not always measured and its evaluation can be difficult.

The isotopic signature of CH_4 can be useful to trace its origin. Using the abacus of Etiope *et al.* (2017), we observe that continental data are consistent with the different

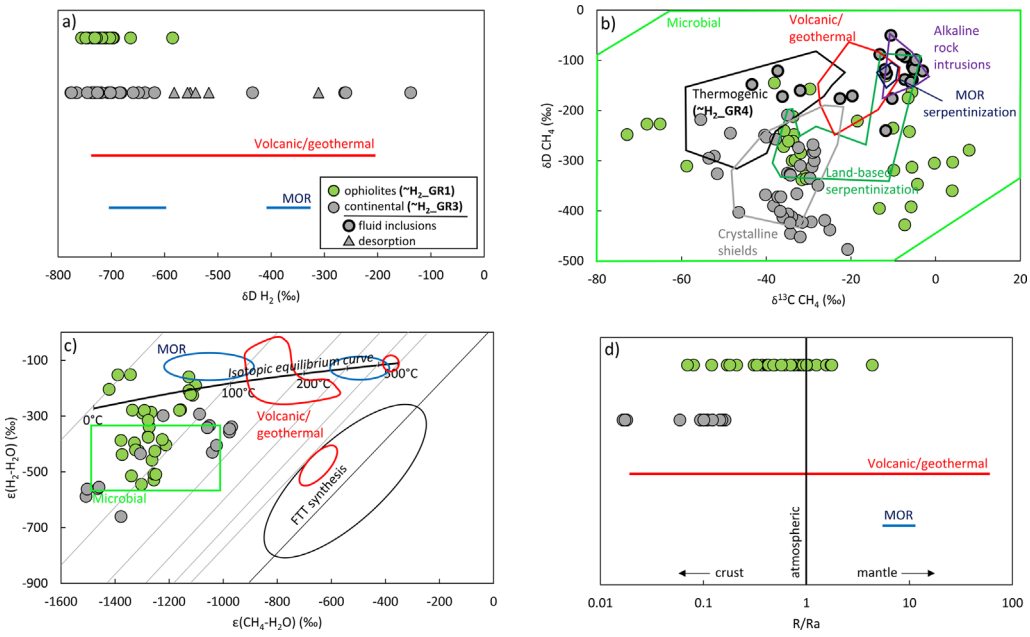

Fig. 17. Isotopic data of H_2-rich gas from ophiolitic, intracontinental represented in different graphs (Abrajano *et al.*, 1988; Etiope *et al.*, 2011; Lévy *et al.*, 2023; Prinzhofer *et al.*, 2018; Randazzo *et al.*, 2021; Sherwood *et al.*, 1988; Sherwood Lollar *et al.*, 1993, 2007, 2008; Truche *et al.*, 2018 Vacquand *et al.*, 2018) compared to MOR (Charlou *et al.*, 1996; Proskurowski *et al.*, 2006, 2008) and volcanic/geothermal data (Arnason, 1977; Caliro *et al.*, 2015; Darling and Talbot, 2003; Kiyosu, 1983; Ricci *et al.*, 2022; Taran *et al.*, 2010). (a) δD of H_2 for the different systems. (b) δD and $\delta^{13}C$ of CH_4. We observe different zones related to a specific source using boundaries from Etiope (2017) and Xia and Gao (2022). (c) ε notation of H_2-H_2O and CH_4-H_2O. This graph is useful to observe if the system is at thermodynamic equilibrium and to use the different couples as geothermometers if possible. (d) The R/Ra ratio allows for defining the crustal or mantellic contributions.

isotopic "boxes". We can note that a gas emanating from a thermogenic source, like H_2_GR4 would plot in the thermogenic area and that some continental data would be consistent with such an origin. Data from the ophiolites does not only show a signature from serpentinization as usually supposed and should be explained by other processes. Xia and Gao (2022) recently showed that mainly all signatures of CH_4 in nature could be obtained by microbial fractionation. The use of this isotopic tool is then to be used with caution to differentiate at first a source.

H_2-H_2O and CH_4-H_2O are two geothermometers usually used to trace the last temperature at which the system isotopically equilibrated (and not a temperature of H_2 generation for example). However, we can only determine a temperature of equilibration when the system is at equilibrium. This can be observed in Figure 17c by the represented isotopic equilibrium curve in a graph combining the isotopic data of H_2, H_2O, and CH_4 using the ε notation (4). If the data do not align with this curve, the system is not at equilibrium. It is mentioned that CH_4-H_2O re-equilibrates slower than the H_2-H_2O system. Therefore, a point out of this trend could reflect the reequilibration of the H_2-H_2O system but not the CH_4-H_2O system which might reflect a higher and more pristine temperature. Some low values of ε(H_2-H_2O) could be associated with microbial activity (Suda *et al.*, 2014).

We globally observe that for most of the compiled data, the temperatures of equilibration are low and mainly out of isotopic equilibrium. This could reflect that the system did not have the necessary time to reequilibrate. This could also be associated with microbial activity.

Finally, the He isotopic composition expressed as R/Ra (5) is presented in Figure 17d. We can distinguish three trends:

- R/Ra = 1: the main contribution of He is atmospheric.
- R/Ra << 1: the main contribution of He is crustal.
- R/Ra >> 1: the main contribution of He is mantellic.

Continental data show a major crustal contribution. The gas from the ophiolites has a variety of isotopic compositions with a contribution from the crust, the mantle, and the atmosphere.

The isotopic data may give important information like the temperature and/or the source. However, especially for H_2, the data have to be interpreted by combining several isotopic systems to be conclusive.

5.2. H_2 generating potential across the different types of H_2_GRs

5.2.1 Case studies of H_2_ GR potential characterization

The assessment of the H_2 potential of H_2_GR is of prime interest because it might decide which geographic

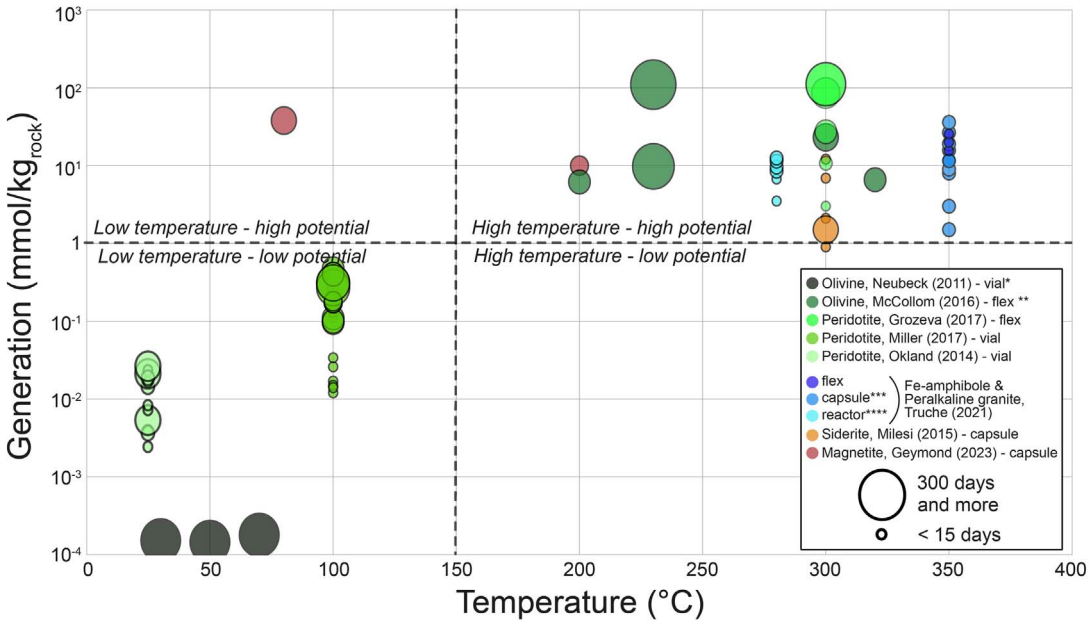

Fig. 18. Experimental H_2 generation after Fe-rich mineral alteration in anoxia, depending on the temperature, and duration of experiment. Note that other experimental parameters may vary such as the reactive surface of the reactant, and water-rock ratio. Please note also that different experimental approaches have been used: *glass vial incubator, **gold flexible bag, ***gold capsule, ****batch reactor with inline sampling device. For further information on the methodology, refer directly to the respective studies (Geymond *et al.*, 2023; Grozeva *et al.*, 2017; McCollom *et al.*, 2016; Milesi *et al.*, 2015; Miller *et al.*, 2017; Neubeck *et al.*, 2011; Okland *et al.*, 2014; Truche *et al.*, 2021).

areas are worth targeting for H_2 exploration. Primarily, the potential of a natural sample is a function of the content of Fe or U, Th, K, or TOC in the rock, which can easily be assessed through laboratory analyses as described previously in Section 4.2. But, the processes involved in H_2 generation are different for each type of H_2_GR.

In the case of water-rock interactions related to H_2 generation, assessing the potential of natural samples is not straightforward because no efficient tool exists yet to rapidly determine the generation potential of a rock by Fe-oxidation (H_2_GR1 and H_2_GR2) or radiolysis (H_2_GR3) from one single analysis. Concerning H_2_GR1 and H_2_GR2 (Fe-oxidation), the potential of rocks often comes from experimental studies, laboriously trying to mimic natural environments by reacting mineral powders and anoxic water. Starting parameters are fully controlled and their evolutions are monitored through time, allowing conclusions to be drawn on H_2 production rates as well as kinetics, which enables extrapolation for geological relevant timeframes. Although all the experimental studies display variability in the approaches and starting parameters, H_2 generations versus temperature are reported in Figure 18. The data plotted are not exhaustive but highlight some important points discussed below:

1. Ultrabasic rocks and associated minerals (*i.e.*, peridotite and olivine) are the most tested reactants (Barbier *et al.*, 2020) because the generation of H_2 was first evidenced during the serpentinization process. However, the few new starting materials tested (pyroxene, amphibole, Fe-carbonates, Fe-oxides) show a comparable H_2 productiveness, which is encouraging in the search for new H_2_GRs around the world.
2. The major part of experimental works has been conducted at elevated temperatures, above 150 °C, probably to reach the optimum temperature for serpentinization, estimated at around 300 °C (Klein *et al.*, 2013; McCollom and Bach, 2009). Various ranges of pressure have been tested, especially in the case of serpentinization. See Barbier *et al.* (2020) for discussion.
3. Subsequently, a limited number of studies have been dedicated to low-temperature alteration but according to the data available in the literature, serpentinization is a low H_2 generator (Neubeck *et al.*, 2011). Observation directly infers that a high-potential material at a high temperature can be a low-potential material at a low temperature and vice versa. Thus, every mineral and rock of interest should probably be tested in both domains of temperature as well as in the presence and absence of catalysts.
4. Finally, although these results must be interpreted cautiously since they result from the alteration of mineral powder rather than cohesive rocks with much lower reactive surface and permeability, redox reactions leading to H_2 generation seem to be a fast process at geological scales. Several mmol.kg$_{rock}^{-1}$ are indeed generated within weeks from these experiments (Fig. 18).

Concerning H_2_GR3 (radiolysis), the generation potential of a rock is mainly evaluated through modeling, using the radioactive element content, the related radioactive decay, and the amount of radiation available (i.e. not removed as heat), as well as the volume of water that may be in contact with the rock. A study aiming to assess the generation rate from this type of H_2_GR3 proposed a value of 0.3–3 $nmol.L^{-1}.y^{-1}$ in Precambrian intracratonic basins such as Witwatersrand in South Africa (Lin *et al.*, 2005), which corresponds to 0.12–1.2 $\mu mol.kg_{rock}^{-1}.My^{-1}$ is based on the chosen porosity.

Concerning H_2_GR4 (late maturation of organic matter), the assessment of the H_2 potential is easier as it is performed by one single analysis conducted on Rock-Eval. In the Songliao and Cooper basins, the maximum H_2-generating potential is similar for organic-rich lacustrine shales and coals, respectively, and was estimated up to 136 $mmol.kg_{rock}^{-1}$ (Horsfield *et al.*, 2022; Mahlstedt *et al.*, 2022). The maximum generation rate was estimated using an Arrhenius law at 6.8 $mmol.kg_{rock}^{-1}.My^{-1}$ at around 250 °C. Early generated H_2 is most likely further reacted with pyrolysis intermediates in nature. Basin modeling is now clearly needed to model the H_2 generation against time and depth (Boreham *et al.*, 2023) and to include the other elements of the H_2 system (i.e., migration, trapping, and preservation).

5.2.2 Questioning the possibility of a common framework to compare all H_2_GR

The methodologies used to quantify the potential of H_2 generation differ from one H_2_GR to another. Maybe the industry will gradually realize that only one of the H_2_GR types generates the majority of accumulations and that the contribution of the others can be neglected. This ranking remains hard to achieve, notably because the geodynamic parameters controlling each type of H_2 generation are different. The role of the temperature, time, and water availability is different and the fact that the retention time in the reservoirs is mainly unknown in many cases makes the problem more complex. As seen in the previous section, Fe-oxidation is dependent on temperature and water circulation, Radiolysis is exclusively dependent on water circulation and remaining TOC is dependent on the initial TOC but also on temperature history. Draw comparisons from the aforementioned case studies remain very qualitative, but two points should be discussed:

1. Concerning the temperature dependency, it is interesting to point out that H_2 can be generated over a wide range of temperatures from both Fe-oxidation and radiolysis, although the degree of Fe-oxidation in minerals will differ depending on the temperature and water availability.
2. Concerning the time scales involved in H_2 generation, intracratonic radiolysis is very slow and the maturation of shales under regular burial rate requires million years to generate µmol to mmol per kg_{rock}. Long-term accumulation under a good seal seems mandatory to constitute economic resources. In parallel, the kinetics of H_2 generation from Fe-oxidation in natural environments is still a matter of debate but seems to be much faster, inferring H_2 could be continuously produced nowadays in favorable environments.

5.3 Model of H_2 accumulation?

The number of case studies is too small to know which type of accumulations will be mainly found. By analogy to other fluids systems in the subsurface, the community mainly thinks in terms of accumulation created by a trap, a reservoir rock, and a seal. In the O&G world, the accumulation may be old with a charge which is considered fossil since there is no recharge at the time scale of the field production. On the opposite, within the geothermal world, the explorations are also looking for a reservoir below a seal but the recharge in hot steam could be fast enough to be adjusted to the production. We believe that H_2 accumulations could be explained using two settings: (i) H_2 dynamic system and (ii) H_2 long-term accumulation. These two models are extremes, and it is likely that reality will often be somewhere in between.

H_2 dynamic system

If the H_2 is generated at a high generation rate (like from H_2_GR1 and H_2_GR2), one may consider the system as a dynamic one. There is no need for a trap but a recent seal would slow down the flow and allows accumulations (Prinzhofer and Cacas-Stentz, 2023). We can take the example of ophiolites, which can produce H_2 at the basis of the sequence where peridotites are fractured and where the formed H_2 is more or less sealed by the impermeable non-fractured peridotite above. It is an optimistic model since the charge of the reservoir could be forever, at a human time scale, but pessimistic in the sense of what has been produced previously is lost.

To constrain the model, more parameters have to be taken into account, like the water migration altering the rocks, through the porosity and the permeability (Karolytė *et al.*, 2022). Moreover, when the water is associated with the gas, its analysis can be relevant, giving information about its age. Based on the geochemical tool used, we can have access to a residence time varying from several months to several million years. This can be very helpful when an H_2 production model has to be built based on the alteration of rocks by the measured water. Moreover, the impact of microbiology on the consumption/production of H_2 has also to be taken into account in the model. For example, the modeling done by (Myagkiy *et al.*, 2020a,b) shows that microbial activity may strongly reduce the H_2 flow at low temperatures. Therefore, the flux is expected to be stronger at depth.

Long-term accumulations

Like in petroleum systems, this model includes an H_2_GR, a trap, a reservoir rock, and a seal. Salt is proven to be a good seal, in the subsurface storage facilities but also at geological time scale. In the Amadeus Basin in central Australia, a Neoproterozoic salt layer seals the CH_4, H_2,

and He-bearing reservoir (Leila *et al.*, 2022). Such a presence in a basin should always be noted (Bradshaw *et al.*, 2023). However, other rocks might behave as a good seal, like in Mali where the accumulation is found below dolerite layers (Prinzhofer *et al.*, 2018), or in Kansas where shales are present (Guélard *et al.*, 2017). To find an accumulation, drilling will be mandatory in combination with acquiring seismic data on the zone of interest. It is worth noting that an accumulation charged by radiolysis, from H_2_GR3, is likely a long-term accumulation since the process is slow and widespread.

5.4 Are the natural H_2 resources promising?

If three H_2_GR are present in the same area, which one ranks first? In our opinion, it is still very difficult to propose a classification of the H_2_GR as well as of the surface indices that will allow us to be more or less optimistic about the H_2 resources in an area. Regarding reserves and proven reserves, it is more uncertain since the number of wells dedicated to H_2 exploration is very low.

Up to now, all the discoveries have been fortuitous looking for water or oil and gas. Finding H_2 without looking for can be seen as very positive, as it infers we should find even more H_2 while looking for it. The case of Mali is interesting, in the sense that around twenty wells drilled since the discovery well also found H_2-rich gas (Diallo *et al.* 2022; Maiga *et al.* 2023).

It is similarly difficult to propose a classification of the critical factors to explore a region. From our experience, each field trip campaign in a selected area resting on pre-field work that targeted the presence of H_2_GR and vegetation index anomalies appeared successful and H_2 was found. It suggests that in many places when a H_2_GR is present at depth together with H_2 surface or subsurface indices, there is an active H_2 release today.

In Mali, there are existing wells with H_2 presence, SCDs, and a Neoproterozoic cratonic area. In the USA, where the exploration is active, H_2_GR, H_2-related SCDs, and old wells with H_2 are all present. Australia is a similar case. In South Australia for instance, old subsurface data already confirmed the presence of H_2, SCDs are numerous, and the craton is iron-rich. Alternatively, when only one single criterion was found during pre-field work, either the presence of an H_2_GR or some SCDs with ambiguous characteristics, field trip results often turned out disappointing.

At the current level of knowledge, or lack thereof, we must certainly remain modest and optimistic and just acquire new data. Soil gas sampling and further gas and rock analyses are globally cheap to acquire and may help to lower the risk in an area. Basin modeling could be done to quantify the water and gas circulation. However, surface indices say nothing about the potential of the area for economic production compared to fully calibrated models.

Various evaluations of the H_2 resources have been published during the last years and this is a recurring question, especially from those who doubt that this resource can change the game. Some authors (Larin *et al.*, 2015; Smith *et al.*, 2005) considered since the beginning that this resource could be major but the first estimates concerning the natural H_2 generation that have been published were globally rather low. They increase recently with the increasing knowledge about natural H_2 generation.

Two global evaluations published in 2020 converged close to 23 Mt/yr (Worman *et al.*, 2020; Zgonnik, 2020), corresponding to a quarter of the current H_2 world consumption.

Worman *et al.* (2020) and co-authors only considered the oceanic domain and estimated that 12 Mt/yr may come from the magma crystallization, about 10 Mt/yr from the serpentinization, and 1 Mt/yr from the radiolysis. Zgonnik (2020) considered that 23 Mt/yr are produced by the MOR and ophiolites and that the radiolysis is almost neglectable (0.38 Mt/yr). This author did not estimate the deep H_2 flow, the primordial H_2 coming from the mantle, and the core degassing, nor the potential generation from the iron-rich sedimentary facies. Both studies considered that the 23 Mt/yr is a lower-bound estimate and, as a fact, only 2 of the 4 H_2_GR described in the present paper were considered. These different authors converge on the fact that processes such as the alteration of basalts, the degassing of magma, the alteration of the oceanic crust at low temperatures, or the pyritization generate lower quantities compared to serpentinization. Again, these estimates were done independently but they were based on the knowledge at that time, or at least a model of H_2 generation admitted as mostly due to serpentinization. H_2_GR2 and H_2_GR4 have now to be taken into account in the global H_2 production models.

For H_2_GR4, the late maturation of coal and organic-rich source rocks, we have to consider resources and reserves as in the O&G industry. For the Songlia Basin (China), the H_2 resources are estimated at 4631 Gt which means about 46,000 yr of the current world consumption (0.1 Gt/yr) (Horsfield *et al.*, 2022). For the Copper Basin in Australia, the resources are estimated at 0.16 Gt (from the coal) and 0.06 Gt (from the shale and coaly shale), so 0.22 Gt (Mahlstedt *et al.*, 2022). These last authors extrapolated these results considering the size and depth of the basin where organic-rich shale has a maturity over VR 3.5% and proposed $3.5\ 10^{12}$ t. The transition from resources to reserves and then to prove reserves will definitively result in a decrease of one or two orders of magnitude, especially if in many cases the H_2 reservoir seal is not perfect (Prinzhofer and Cacas-Stentz, 2023) but these numbers highlight the fact that the natural H_2 resource is there. The community no longer has to argue about whether this resource is available, but rather where H_2 is currently accumulated and/or where the flow is large enough to allow production.

Supplementary material

Supplementary materials are available at https://doi.org/10.2516/stet/2023021/olm

- Database of the soil gas analyses done in the various case studies.
- Major gas data plotted Figure 16.
- Isotopic data plotted Figure 17.

Acknowledgments. We acknowledge O. Sissmann (*IFPen*) for many interesting discussions on H_2 and their help in data

collection. We thank C. Rigollet and the CVA H_2 team for their support for the acquisition in Nouvelle Aquitaine and in Djibouti.

References

Abrajano T.A., Sturchio N.C., Bohlke J.K., Lyon G.L., Poreda R. J., Stevens C.M. (1988) Methane-hydrogen gas seeps, Zambales Ophiolite, Philippines: Deep or shallow origin? *Chem. Geol.* **71**, 1–3, 211–222. https://doi.org/10.1016/0009-2541(88)90116-7.

Aftabi A., Atapour H., Mohseni S., Babaki A. (2021) Geochemical discrimination among different types of banded iron formations (BIFs): A comparative review, *Ore Geol. Rev.* **136**, 104244. https://doi.org/10.1016/j.oregeorev.2021.104244.

Arnason B. (1977) The hydrogen-water isotope thermometer applied to geothermal areas in Iceland, *Geothermics* **5**, 1, 75–80. https://doi.org/10.1016/0375-6505(77)90011-6.

Ballentine C.J., Burnard P.G. (2002) Production, release and transport of noble gases in the continental crust, *Rev. Mineral. Geochem.* **47**, 1, 481–538. https://doi.org/10.2138/rmg.2002.47.12.

Barbier S., Huang F., Andreani M., Tao R., Hao J., Eleish A., Prabhu A., Minhas O., Fontaine K., Fox P., Daniel I. (2020) A review of H_2, CH_4, and hydrocarbon formation in experimental serpentinization using network analysis, *Front. Earth Sci.* **8**, 209. https://doi.org/10.3389/feart.2020.00209.

Barnes I., Lamarche V.C., Himmelberg G. (1967) Geochemical evidence of present-day serpentinization, *Science* **156**, 3776, 830–832. https://doi.org/10.1126/science.156.3776.830.

Behar F., Beaumont V., Penteado H.L.D.B. (2001) Rock-Eval 6 technology: performances and Developments, *Oil Gas Sci. Technol.* **56**, 2, 111–134. https://doi.org/10.2516/ogst:2001013.

Boreham C.J., Edwards D.S., Czado K., Rollet N., Wang L., Van Der Wielen S., Champion D., Blewett R., Feitz A., Henson P. A. (2021) Hydrogen in Australian natural gas: Occurrences, sources and resources, *APPEA J.* **61**, 1, 163. https://doi.org/10.1071/AJ20044.

Boreham C.J., Edwards D.S., Feitz A.J., Murray A.P., Mahlstedt N., Horsfield B., Boreham C.J., Edwards D.S., Feitz A.J., Murray A.P., Mahlstedt N., Horsfield B. (2023) Modelling of hydrogen gas generation from overmature organic matter in the Cooper Basin, Australia, *APPEA J.* **63**, 2, S351–S356. https://doi.org/10.1071/AJ22084.

Bradshaw M., Rees S., Wang L., Szczepaniak M., Cook W., Voegeli S., Boreham C., Wainman C., Wong S., Southby C., Feitz A., Bradshaw M., Rees S., Wang L., Szczepaniak M., Cook W., Voegeli S., Boreham C., Wainman C., Wong S., Southby C., Feitz A. (2023) Australian salt basins – options for underground hydrogen storage, *APPEA J.* **63**, 1, 285–304. https://doi.org/10.1071/AJ22153.

Caliro S., Viveiros F., Chiodini G., Ferreira T. (2015) Gas geochemistry of hydrothermal fluids of the S. Miguel and Terceira Islands, Azores, *Geochim. Cosmochim. Acta* **168**, 43–57. https://doi.org/10.1016/j.gca.2015.07.009.

Cathles L., Prinzhofer A. (2020) What pulsating H_2 emissions suggest about the H_2 resource in the Sao Francisco Basin of Brazil, *Geosciences* **10**, 4, 149. https://doi.org/10.3390/geosciences10040149.

Charlou J.L., Donval J.P., Jean-Baptiste P., Dapoigny A., Rona P.A. (1996) Gases and helium isotopes in high temperature solutions sampled before and after ODP Leg 158 drilling at TAG Hydrothermal Field (26 N, MAR), *Geophys. Res. Lett.* **23**, 23, 3491–3494. https://doi.org/10.1029/96GL02141.

Chavagnac V., Monnin C., Ceuleneer G., Boulart C., Hoareau G. (2013) Characterization of hyperalkaline fluids produced by low-temperature serpentinization of mantle peridotites in the Oman and Ligurian ophiolites, *Geochem. Geophys. Geosyst.* **14**, 7, 2496–2522. https://doi.org/10.1002/ggge.20147.

Combaudon V., Moretti I., Kleine B.I., Stefánsson A. (2022) Hydrogen emissions from hydrothermal in Iceland and comparison with the Mid-Atlantic Ridge, *Int. J. Hydrog. Energy.* https://doi.org/10.1016/j.ijhydene.2022.01.101.

Coveney R.M., Goebel E.D., Zeller E.J., Dreschhoff G.A.M., Angino E.E. (1987) Serpentinization and the origin of hydrogen gas in Kansas, *Am. Assoc. Pet. Geol. Bull.* **71**, 1, 39–48. https://doi.org/10.1306/94886D3F-1704-11D7-8645000102C1865D.

Cox G.W. (1987) The origin of vegetation circles on stony soils of the Namib Desert near Gobabeb, South West Africa/Namibia, *J. Arid Environ.* **13**, 3, 237–243. https://doi.org/10.1016/S0140-1963(18)31112-1.

Darling W.G., Talbot J.C. (2003) The O & H stable isotopic composition of fresh waters in the British Isles. 1. Rainfall, *Hydrol. Earth Syst. Sci.* **7**, 2, 163–182.

Deville E., Prinzhofer A. (2016) The origin of N_2-H_2-CH_4-rich natural gas seepages in ophiolitic context: a major and noble gases study of fluid seepages in New Caledonia, *Chem. Geol.* **440**, 139–147. https://doi.org/10.1016/j.chemgeo.2016.06.011.

Diallo A., Cissé C.S.T., Lemay J., Brière D.J. (2022) La découverte de l'hydrogène naturel par Hydroma, un « Game Changer » pour la transition énergétique, *Annales des Mines – Réalités industrielles* **2022**, 4, 154–160. https://doi.org/10.3917/rindu1.224.0154.

Espitalie J., Madec M., Tissot B. (1980) Role of mineral matrix in kerogen pyrolysis: Influence on petroleum generation and migration, *Am. Assoc. Pet. Geol. Bull.* **64**, 59–66. https://doi.org/10.1306/2F918928-16CE-11D7-8645000102C1865D.

Etiope G. (2017) Abiotic methane in continental serpentinization sites: An overview, *Procedia Earth Planet. Sci.* **17**, 9–12. https://doi.org/10.1016/j.proeps.2016.12.006.

Etiope G. (2023) Massive release of natural hydrogen from a geological seep (Chimaera, Turkey): Gas advection as a proxy of subsurface gas migration and pressurised accumulations, *Int. J. Hydrog. Energy* **48**, 25, 9172–9184. https://doi.org/10.1016/j.ijhydene.2022.12.025.

Etiope G., Schoell M., Hosgörmez H. (2011) Abiotic methane flux from the Chimaera seep and Tekirova ophiolites (Turkey): Understanding gas exhalation from low temperature serpentinization and implications for Mars, *Earth Planet. Sci. Lett.* **310**, 1–2, 96–104. https://doi.org/10.1016/j.epsl.2011.08.001.

Etiope G., Vadillo I., Whiticar M.J., Marques J.M., Carreira P. M., Tiago I., Benavente J., Jiménez P., Urresti B. (2016) Abiotic methane seepage in the Ronda peridotite massif, southern Spain, *Appl. Geochem.* **66**, 101–113. https://doi.org/10.1016/j.apgeochem.2015.12.001.

Etiope G., Samardžić N., Grassa F., Hrvatović H., Miošić N., Skopljak F. (2017) Methane and hydrogen in hyperalkaline groundwaters of the serpentinized Dinaride ophiolite belt, Bosnia and Herzegovina, *Appl. Geochem.* **84**, 286–296. https://doi.org/10.1016/j.apgeochem.2017.07.006.

Firstov P.P., Shirokov V.A. (2005) Dynamics of molecular hydrogen and its relation to deformational processes at the Petropavlovsk-Kamchatskii geodynamic test site: Evidence from observations in 1999–2003, *Geochem. Int.* **43**, 11, 1056–1064.

Frery E., Langhi L., Maison M., Moretti I. (2021) Natural hydrogen seeps identified in the North Perth Basin, Western Australia, *Int. J. Hydrog. Energy* **46**, 61, 31158–31173. https://doi.org/10.1016/j.ijhydene.2021.07.023.

Furnes H., Dilek Y., de Wit M. (2015) Precambrian greenstone sequences represent different ophiolite types, *Gondwana Res.* **27**, 2, 649–685. https://doi.org/10.1016/j.gr.2013.06.004.

Gaucher E., Moretti I., Pélissier N., Burridge G., Gonthier N. (2023) The place of natural hydrogen in the energy transition: A position paper, *Eur. Geol.* **55**, 5–9.

Geymond U., Ramanaidou E., Lévy D., Ouaya A., Moretti I. (2022) Can weathering of banded iron formations generate natural hydrogen? Evidence from Australia, Brazil and South Africa, *Minerals* **12**, 2, 163. https://doi.org/10.3390/min12020163.

Geymond U., Briolet T., Combaudon V., Sissmann O., Martinez I., Duttine M., Moretti I. (2023) Reassessing the role of magnetite during natural hydrogen generation, *Front. Earth Sci.* **11**, 1169356. https://doi.org/10.3389/feart.2023.1169356.

Grozeva N.G., Klein F., Seewald J.S., Sylva S.P. (2017) Experimental study of carbonate formation in oceanic peridotite, *Geochim. Cosmochim. Acta* **199**, 264–286. https://doi.org/10.1016/j.gca.2016.10.052.

Guélard J., Beaumont V., Rouchon V., Guyot F., Pillot D., Jézéquel D., Ader M., Newell K.D., Deville E. (2017) Natural H_2 in Kansas: Deep or shallow origin?, *Geochem. Geophys. Geosyst.* **18**, 5, 1841–1865. https://doi.org/10.1002/2016GC006544.

Halford D.T., Karolytė R., Barry P.H., Whyte C.J., Darrah T. H., Cuzella J.J., Sonnenberg S.A., Ballentine C.J. (2022) High helium reservoirs in the Four Corners area of the Colorado Plateau, *USA. Chem. Geol.* **596**, 120790. https://doi.org/10.1016/j.chemgeo.2022.120790.

Hirose T., Kawagucci S., Suzuki K. (2011) Mechanoradical H_2 generation during simulated faulting: Implications for an earthquake-driven subsurface biosphere, *Geophys. Res. Lett.* **38**, 17, L17303. https://doi.org/10.1029/2011GL048850.

Horibe Y., Craig H. (1995) D/H fractionation in the system methane-hydrogen-water, *Geochim. Cosmochim. Acta* **59**, 24, 5209–5217. https://doi.org/10.1016/0016-7037(95)00391-6.

Horsfield B., Mahlstedt N., Weniger P., Misch D., Vranjes-Wessely S., Han S., Wang C. (2022) Molecular hydrogen from organic sources in the deep Songliao Basin, *PR China. Int. J. Hydrog. Energy* **47**, 38, 16750–16774. https://doi.org/10.1016/j.ijhydene.2022.02.208.

Karolytė R., Warr O., van Heerden E., Flude S., de Lange F., Webb S., Ballentine C.J., Sherwood Lollar B. (2022) The role of porosity in H_2/He production ratios in fracture fluids from the Witwatersrand Basin, South Africa, *Chem. Geol.* **595**, 120788. https://doi.org/10.1016/j.chemgeo.2022.120788.

Kiyosu Y. (1983) Hydrogen isotopic compositions of hydrogen and methane from some volcanic areas in northeastern Japan, *Earth Planet. Sci. Lett.* **62**, 1, 41–52. https://doi.org/10.1016/0012-821X(83)90069-9.

Klein F., Bach W., McCollom T.M. (2013) Compositional controls on hydrogen generation during serpentinization of ultramafic rocks, *Lithos* **178**, 55–69. https://doi.org/10.1016/j.lithos.2013.03.008.

Klein F., Marschall H.R., Bowring S.A., Humphris S.E., Horning G. (2017) Mid-ocean ridge serpentinite in the Puerto Rico Trench: From seafloor spreading to subduction, *J. Petrol.* **58**, 9, 1729–1754. https://doi.org/10.1093/petrology/egx071.

Klein F., Grozeva N.G., Seewald J.S. (2019) Abiotic methane synthesis and serpentinization in olivine-hosted fluid inclusions, *Proc. Natl. Acad. Sci* **116**, 36, 17666–17672. https://doi.org/10.1073/pnas.1907871116.

Larin N., Zgonnik V., Rodina S., Deville E., Prinzhofer A., Larin V.N. (2015) Natural molecular hydrogen seepage associated with surficial, rounded depressions on the European Craton in Russia, *Nat. Resour. Res.* **24**, 3, 369–383. https://doi.org/10.1007/s11053-014-9257-5.

Lefeuvre N., Truche L., Donzé F.-V., Ducoux M., Barré G., Fakoury R.-A., Calassou S., Gaucher E.C. (2021) Native H_2 exploration in the Western Pyrenean Foothills, *Geochem. Geophys. Geosyst.* **22**, 8, e2021GC009917. https://doi.org/10.1029/2021GC009917.

Lefeuvre N., Truche L., Donzé F.-V., Gal F., Tremosa J., Fakoury R.-A., Calassou S., Gaucher E.C. (2022) Natural hydrogen migration along thrust faults in foothill basins: The North Pyrenean Frontal Thrust case study, *Appl. Geochem.* **145**, 105396. https://doi.org/10.1016/j.apgeochem.2022.105396.

Leila M., Lévy D., Battani A., Piccardi L., Šegvić B., Badurina L., Pasquet G., Combaudon V., Moretti I. (2021) Origin of continuous hydrogen flux in gas manifestations at the Larderello geothermal field, Central Italy, *Chem. Geol.* **585**, 120564. https://doi.org/10.1016/j.chemgeo.2021.120564.

Leila M., Loiseau K., Moretti I. (2022) Controls on generation and accumulation of blended gases (CH_4/H_2/He) in the Neoproterozoic Amadeus Basin, *Australia. Mar. Pet. Geol.* **140**, 105643. https://doi.org/10.1016/j.marpetgeo.2022.105643.

Lévy D., Callot J.-P., Moretti I., Duttine M., Dubreuil B., De Parseval P., Boudouma O. (2022) Successive phases of serpentinization and carbonation recorded in the Sivas ophiolite (Turkey), from oceanic crust accretion to post-obduction alteration, *BSGF – Earth Sci. Bull.* **193**, 12. https://doi.org/10.1051/bsgf/2022015.

Lévy D., Boka-Mene M., Meshi A., Fejza I., Guermont T., Hauville B., Pelissier N. (2023) Looking for natural hydrogen in Albania and Kosova, *Front. Earth Sci.* **11**, 1167634. https://doi.org/10.3389/feart.2023.1167634.

Lopez-Lazaro C., Bachaud P., Moretti I., Ferrando N. (2019) Predicting the phase behavior of hydrogen in NaCl brines by molecular simulation for geological applications, *BSGF – Earth Sci. Bull.* **190**, 7. https://doi.org/10.1051/bsgf/2019008.

Lin L.-H., Hall J., Lippmann-Pipke J., Ward J., Lollar B., Deflaun M., Rothmel R., Moser D., Gihring T., Mislowack B., Onstott T. (2005) Radiolytic H_2 in continental crust: Nuclear power for deep subsurface microbial communities, *Geochem. Geophys. Geosyst.* **6**, Q07003. https://doi.org/10.1029/2004GC000907.

Mahlstedt N., Horsfield B., Weniger P., Misch D., Shi X., Noah M., Boreham C. (2022) Molecular hydrogen from organic sources in geological systems, *J. Nat. Gas Sci. Eng.* **105**, 104704. https://doi.org/10.1016/j.jngse.2022.104704.

Maiga O., Deville E., Laval J., Prinzhofer A., Diallo A.B. (2023) Characterization of the spontaneously recharging natural hydrogen reservoirs of Bourakebougou in Mali, *Sci. Rep.* **13**, 1, 11876. https://doi.org/10.1038/s41598-023-38977-y.

Malvoisin B., Brunet F. (2023) Barren ground depressions, natural H_2 and orogenic gold deposits: Spatial link and geochemical model, *Sci. Total Environ.* **856**, 158969. https://doi.org/10.1016/j.scitotenv.2022.158969.

Martín-Hernández F., Lüneburg C.M., Aubourg C., Jackson M. (2004) Magnetic fabric: Methods and applications – an introduction, *Geol. Soc. Spec. Publ.* **238**, 1–7. https://doi.org/10.1144/GSL.SP.2004.238.01.01.

McCollom T.M., Bach W. (2009) Thermodynamic constraints on hydrogen generation during serpentinization of ultramafic rocks, *Geochim. Cosmochim. Acta* **73**, 3, 856–875. https://doi.org/10.1016/j.gca.2008.10.032.

McCollom T.M., Klein F., Robbins M., Moskowitz B., Berquó T.S., Jöns N., Bach W., Templeton A. (2016) Temperature trends for reaction rates, hydrogen generation, and partitioning of iron during experimental serpentinization of olivine, *Geochim. Cosmochim. Acta* **181**, 175–200. https://doi.org/10.1016/j.gca.2016.03.002.

Mével C. (2003) Serpentinization of abyssal peridotites at mid-ocean ridges, *CR Geosci.* **335**, 10, 825–852. https://doi.org/10.1016/j.crte.2003.08.006.

Milesi V., Guyot F., Brunet F., Richard L., Recham N., Benedetti M., Dairou J., Prinzhofer A. (2015) Formation of CO_2, H_2 and condensed carbon from siderite dissolution in the 200–300 °C range and at 50 MPa, *Geochim. Cosmochim. Acta* **154**, 201–211. https://doi.org/10.1016/j.gca.2015.01.015.

Miller H.M., Mayhew L.E., Ellison E.T., Kelemen P., Kubo M., Templeton A.S. (2017) Low temperature hydrogen production during experimental hydration of partially-serpentinized dunite, *Geochim. Cosmochim. Acta* **209**, 161–183. https://doi.org/10.1016/j.gca.2017.04.022.

Moretti I., Brouilly E., Loiseau K., Prinzhofer A., Deville E. (2021a) Hydrogen emanations in intracratonic areas: New guide lines for early exploration basin screening, *Geosciences* **11**, 3, 145. https://doi.org/10.3390/geosciences11030145.

Moretti I., Prinzhofer A., Françolin J., Pacheco C., Rosanne M., Rupin F., Mertens J. (2021b) Long-term monitoring of natural hydrogen superficial emissions in a Brazilian cratonic environment. Sporadic large pulses versus daily periodic emissions, *Int. J. Hydrog. Energy* **46**, 5, 3615–3628. https://doi.org/10.1016/j.ijhydene.2020.11.026.

Moretti I., Geymond U., Pasquet G., Aimar L., Rabaute A. (2022) Natural hydrogen emanations in Namibia: Field acquisition and vegetation indexes from multispectral satellite image analysis, *Int. J. Hydrog. Energy* **47**, 84, 35588–35607. https://doi.org/10.1016/j.ijhydene.2022.08.135.

Moretti I., Baby P., Alvarez Zapata P., Mendoza R.V. (2023) Subduction and hydrogen release: The case of Bolivian Altiplano, *Geosciences* **13**, 4, 109. https://doi.org/10.3390/geosciences13040109.

Myagkiy A., Brunet F., Popov C., Krüger R., Guimarães H., Sousa R.S., Charlet L., Moretti I. (2020a) H_2 dynamics in the soil of a H_2-emitting zone (São Francisco Basin, Brazil): Microbial uptake quantification and reactive transport modelling, *Appl. Geochem.* **112**, 104474. https://doi.org/10.1016/j.apgeochem.2019.104474.

Myagkiy A., Moretti I., Brunet F. (2020b) Space and time distribution of subsurface H_2 concentration in so-called "fairy circles": Insight from a conceptual 2-D transport model, *BSGF – Earth Sci. Bull.* **191**, 13. https://doi.org/10.1051/bsgf/2020010.

Neal C., Stanger G. (1983) Hydrogen generation from mantle source rocks in Oman, *Earth Planet. Sci. Lett.* **66**, 315–320. https://doi.org/10.1016/0012-821X(83)90144-9.

Neubeck A., Duc N.T., Bastviken D., Crill P., Holm N.G. (2011) Formation of H_2 and CH_4 by weathering of olivine at temperatures between 30 and 70 °C, *Geochem. Trans.* **12**, 1, 6. https://doi.org/10.1186/1467-4866-12-6.

Nivin V.A. (2019) Occurrence forms, composition, distribution, origin and potential hazard of natural hydrogen–hydrocarbon gases in ore deposits of the Khibiny and Lovozero Massifs: A Review, *Minerals* **9**, 9, 535. https://doi.org/10.3390/min9090535.

Okland I., Huang S., Thorseth I.H., Pedersen R.B. (2014) Formation of H_2, CH_4 and N-species during low-temperature experimental alteration of ultramafic rocks, *Chem. Geol.* **387**, 22–34. https://doi.org/10.1016/j.chemgeo.2014.08.003.

Pasquet G., Houssein Hassan R., Sissmann O., Varet J., Moretti I. (2021) An attempt to study natural H_2 resources across an oceanic ridge penetrating a continent: The Asal-Ghoubbet Rift (Republic of Djibouti), *Geosciences* **12**, 1, 16. https://doi.org/10.3390/geosciences12010016.

Pasquet G., Idriss A.M., Ronjon-Magand L., Ranchou-Peyruse M., Guignard M., Duttine M., Ranchou-Peyruse A., Moretti I. (2023) Natural hydrogen potential and basaltic alteration in the Asal-Ghoubbet rift, Republic of Djibouti, *BSGF – Earth Sci. Bull.* **194**, 9. https://doi.org/10.1051/bsgf/2023004.

Potter J., Salvi S., Longstaffe F.J. (2013) Abiogenic hydrocarbon isotopic signatures in granitic rocks: Identifying pathways of formation, *Lithos* **182–183**, 114–124. https://doi.org/10.1016/j.lithos.2013.10.001.

Prinzhofer A., Cacas-Stentz M.-C. (2023) Natural hydrogen and blend gas: a dynamic model of accumulation, *Int. J. Hydrog. Energy* **48**, 57, 21610–21623. https://doi.org/10.1016/j.ijhydene.2023.03.060.

Prinzhofer A., Tahara Cissé C.S., Diallo A.B. (2018) Discovery of a large accumulation of natural hydrogen in Bourakebougou (Mali), *Int. J. Hydrog. Energy* **43**, 42, 19315–19326. https://doi.org/10.1016/j.ijhydene.2018.08.193.

Prinzhofer A., Moretti I., Françolin J., Pacheco C., D'Agostino A., Werly J., Rupin F. (2019) Natural hydrogen con tinuous emission from sedimentary basins: The example of a Brazilian H_2-emitting structure, *Int. J. Hydrog. Energy* **44**, 12, 5676–5685. https://doi.org/10.1016/j.ijhydene.2019. 01.119.

Proskurowski G., Lilley M.D., Kelley D.S., Olson E.J. (2006) Low temperature volatile production at the Lost City Hydrothermal Field, evidence from a hydrogen stable isotope geothermometer, *Chem. Geol.* **229**, 4, 331–343. https://doi.org/10.1016/j.chemgeo.2005.11.005.

Proskurowski G., Lilley M.D., Seewald J.S., Früh-Green G.L., Olson E.J., Lupton J.E., Sylva S.P., Kelley D.S. (2008) Abiogenic hydrocarbon production at Lost City Hydrothermal Field, *Science* **319**, 5863, 604–607. https://doi.org/10.1126/science.1151194.

Randazzo P., Caracausi A., Aiuppa A., Cardellini C., Chiodini G., D'Alessandro W., Li Vigni L., Papic P., Marinkovic G., Ionescu A. (2021) Active degassing of deeply sourced fluids in central Europe: New evidences from a geochemical study in Serbia, *Geochem. Geophys. Geosyst.* **22**, 11, e2021GC010017. https://doi.org/10.1029/2021GC010017.

Ricci A., Kleine B.I., Fiebig J., Gunnarsson-Robin J., Mativo Kamunya K., Mountain B., Stefánsson A. (2022) Equilibrium and kinetic controls on molecular hydrogen abundance and hydrogen isotope fractionation in hydrothermal fluids, *Earth Planet. Sci. Lett.* **579**, 117338. https://doi.org/10.1016/j.epsl.2021.117338.

Rigollet C., Prinzhofer A. (2022) Natural hydrogen: A new source of carbon-free and renewable energy that can compete with hydrocarbons, *First Break* **40**, 10, 78–84. https://doi.org/10.3997/1365-2397.fb2022087.

Rochette P., Ellert B., Gregorich E.G., Desjardins R.L., Pattey E., Lessard R., Johnson B.G. (1997) Description of a dynamic closed chamber for measuring soil respiration and its comparison

with other techniques, *Can. J. Soil Sci.* **77**, 2, 195–203. https://doi.org/10.4141/S96-110.

Rosanne M. (2020). PARHyS System: A new approach to H_2 concentration measurements in the subsurface, in: 27e édition de la Réunion des Sciences de la Terre, Lyon, 2021.

Salvi S., Williams-Jones A.E. (1997) Fischer-Tropsch synthesis of hydrocarbons during sub-solidus alteration of the Strange Lake peralkaline granite, Quebec/Labrador, Canada, *Geochim. Cosmochim. Acta* **61**, 1, 83–99. https://doi.org/10.1016/S0016-7037(96)00313-4.

Sato M., Sutton A.J., McGee K.A., Russell-Robinson S. (1986) Monitoring of hydrogen along the San Andreas and Calaveras faults in central California in 1980–1984, *J. Geophys. Res. Solid Earth* **91**, B12, 12315–12326. https://doi.org/10.1029/JB091iB12p12315.

Sherwood B., Fritz P., Frape S.K., Macko S.A., Weise S.M., Welhan J.A. (1988) Methane occurrences in the Canadian Shield, *Chem. Geol.* **71**, 1–3, 223–236. https://doi.org/10.1016/0009-2541(88)90117-9.

Sherwood Lollar B., Frape S.K., Fritz P., Macko S.A., Welhan J.A., Blomqvist R., Lahermo P.W. (1993) Evidence for bacterially generated hydrocarbon gas in Canadian shield and fennoscandian shield rocks, *Geochim. Cosmochim. Acta* **57**, 23–24, 5073–5085. https://doi.org/10.1016/0016-7037(93)90609-Z.

Sherwood Lollar B., Lacrampe-Couloume G., Slater G.F., Ward J., Moser D.P., Gihring T.M., Lin L.-H., Onstott T.C. (2006) Unravelling abiogenic and biogenic sources of methane in the Earth's deep subsurface, *Chem. Geol.* **226**, 3–4, 328–339. https://doi.org/10.1016/j.chemgeo.2005.09.027.

Sherwood Lollar B., Voglesonger K., Lin L.-H., Lacrampe-Couloume G., Telling J., Abrajano T.A., Onstott T.C., Pratt L.M. (2007) Hydrogeologic controls on episodic H_2 release from precambrian fractured rocks – energy for deep subsurface life on Earth and Mars, *Astrobiology* **7**, 6, 971–986. https://doi.org/10.1089/ast.2006.0096.

Sherwood Lollar B., Lacrampe-Couloume G., Voglesonger K., Onstott T.C., Pratt L.M., Slater G.F. (2008) Isotopic signatures of CH_4 and higher hydrocarbon gases from Precambrian Shield sites: A model for abiogenic polymerization of hydrocarbons, *Geochim. Cosmochim. Acta* **72**, 19, 4778–4795. https://doi.org/10.1016/j.gca.2008.07.004.

Simon J., Fulton P., Prinzhofer A., Cathles L. (2020) Earth tides and H_2 venting in the Sao Francisco Basin, Brazil, *Geosciences* **10**, 10, 414. https://doi.org/10.3390/geosciences10100414.

Smith N.J.P., Shepherd T.J., Styles M.T., Williams G.M. (2005) Hydrogen exploration: A review of global hydrogen accumulations and implications for prospective areas in NW Europe, *Geol. Soc. London Pet. Geol. Conf.* **6**, 1, 349–358. https://doi.org/10.1144/0060349.

Suda K., Ueno Y., Yoshizaki M., Nakamura H., Kurokawa K., Nishiyama E., Yoshino K., Hongoh Y., Kawachi K., Omori S., Yamada K., Yoshida N., Maruyama S. (2014) Origin of methane in serpentinite-hosted hydrothermal systems: The CH_4–H_2–H_2O hydrogen isotope systematics of the Hakuba Happo hot spring, *Earth Planet. Sci. Lett.* **386**, 112–125. https://doi.org/10.1016/j.epsl.2013.11.001.

Suzuki N., Saito H., Hoshino T. (2017) Hydrogen gas of organic origin in shales and metapelites, *Int. J. Coal Geol.* **173**, 227–236. https://doi.org/10.1016/j.coal.2017.02.014.

Taran Y.A., Varley N.R., Inguaggiato S., Cienfuegos E. (2010) Geochemistry of H_2- and CH_4-enriched hydrothermal fluids of Socorro Island, Revillagigedo Archipelago, Mexico. Evidence for serpentinization and abiogenic methane: Socorro hydrocarbons, *Geofluids* **10**, 4, 542–555. https://doi.org/10.1111/j.1468-8123.2010.00314.x.

Theron G.K. (1979) Die verskynsel van kaal kolle in Kaokoland, Suidwes-Afrika, *J. South African Biol. Soc.* **20**, 43–53.

Tinley K.L. (1971) Etosha and the Kaokoveld, *Afr. J. Wildl. Res.* **25**, 1–16.

Truche L., Joubert G., Dargent M., Martz P., Cathelineau M., Rigaudier T., Quirt D. (2018) Clay minerals trap hydrogen in the Earth's crust: Evidence from the Cigar Lake uranium deposit, Athabasca, *Earth Planet. Sci. Lett.* **493**, 186–197. https://doi.org/10.1016/j.epsl.2018.04.038.

Truche L., McCollom T.M., Martinez I. (2020) Hydrogen and abiotic hydrocarbons: Molecules that change the world, *Elements* **16**, 1, 13–18. https://doi.org/10.2138/gselements.16.1.13.

Truche L., Bourdelle F., Salvi S., Lefeuvre N., Zug A., Lloret E. (2021) Hydrogen generation during hydrothermal alteration of peralkaline granite, *Geochim. Cosmochim. Acta* **308**, 42–59. https://doi.org/10.1016/j.gca.2021.05.048.

Vacquand C., Deville E., Beaumont V., Guyot F., Sissmann O., Pillot D., Arcilla C., Prinzhofer A. (2018) Reduced gas seepages in ophiolitic complexes: Evidences for multiple origins of the H_2-CH_4-N_2 gas mixtures, *Geochim. Cosmochim. Acta* **223**, 437–461. https://doi.org/10.1016/j.gca.2017.12.018.

Vaughan A.P.M., Scarrow J.H. (2003) Ophiolite obduction pulses as a proxy indicator of superplume events?, *Earth Planet. Sci. Lett.* **213**, 3, 407–416. https://doi.org/10.1016/S0012-821X(03)00330-3.

Wagner S.W., Reicosky D.C., Alessi R.S. (1997) Regression models for calculating gas fluxes measured with a closed chamber, *Agron. J.* **89**, 2, 279–284. https://doi.org/10.2134/agronj1997.00021962008900020021x.

Ward L.K. (1933) Inflammable gases occluded in the prepalaezoic rocks of South Australia, *Trans. R. Soc. S. Aust.* **57**, 42–47.

Worman S.L., Pratson L.F., Karson J.A., Schlesinger W.H. (2020) Abiotic hydrogen (H_2) sources and sinks near the Mid-Ocean Ridge (MOR) with implications for the subseafloor biosphere, *Proc. Natl. Acad. Sci.* **117**, 24, 13283–13293. https://doi.org/10.1073/pnas.2002619117.

Xia X., Gao Y. (2022) Validity of geochemical signatures of abiotic hydrocarbon gases on Earth, *J. Geol. Soc.* **179**, 3, jgs2021-077. https://doi.org/10.1144/jgs2021-077.

Yan J., Liu M., Feng Z., Bai Z., Shui H., Li Z., Lei Z., Wang Z., Ren S., Kang S., Yan H. (2020) Study on the pyrolysis kinetics of low-medium rank coals with distributed activation energy model, *Fuel* **261**, 116359. https://doi.org/10.1016/j.fuel.2019.116359.

Zgonnik V. (2020) The occurrence and geoscience of natural hydrogen: A comprehensive review, *Earth Sci. Rev.* **203**, 103140. https://doi.org/10.1016/j.earscirev.2020.103140.

Zgonnik V., Beaumont V., Deville E., Larin N., Pillot D., Farrell K.M. (2015) Evidence for natural molecular hydrogen seepage associated with Carolina bays (surficial, ovoid depressions on the Atlantic Coastal Plain, Province of the USA), *Prog. Earth Planet. Sci.* **2**, 1, 31. https://doi.org/10.1186/s40645-015-0062-5.

Zhang Q., Grohmann S., Xu X., Littke R. (2020) Depositional environment and thermal maturity of the coal-bearing Longtan Shale in southwest Guizhou, China: Implications for shale gas resource potential, *Int. J. Coal Geol.* **231**, 103607. https://doi.org/10.1016/j.coal.2020.103607.

Appendix A

Minerals at the origin of the generation of H_2 from H_2_GR

Olivine

Olivine $(Mg,Fe)_2SiO_4$ is by far the most studied mineral for the assessment of natural H_2 potential since the discovery of H_2 flows at Mid Oceanic Ridges and later in ophiolitic context. Olivine consists in a solid solution between its ferrous and magnesian endmembers: fayalite (Fe_2SiO_4) and forsterite (Mg_2SiO_4), respectively. Olivine is highly present in ultrabasic and basic rocks. Peridotites are generally enriched in forsterite. Concerning the H_2 potential of olivine, fayalite is the endmember of interest, as it carries the Fe^{2+} susceptible to be oxidized. Its alteration during hydrothermal alteration, called serpentinization, leads to the oxidation of Fe and reduction of H_2O to form H_2. A wide range of temperature is favorable for H_2-forming serpentinization, up to >400 °C and down to <100 °C, with an optimum determined around 300 °C (Klein *et al.*, 2013). Secondary minerals formed during serpentinization differ along with the temperature, from magnetite and Mg-serpentine at $T > 200$ °C to Fe-serpentine at $T < 200$ °C.

$$6\left(Mg,Fe^{2+}\right)_2SiO_4 + 7H_2O \rightarrow 3\left(Mg,Fe^{2+,3+}\right)_3Si_2O_5(OH)_4 + Fe^{2+}Fe^{3+}{}_2O_4 + H_2. \quad (A.1)$$

Pyroxene

Pyroxenes, such as olivine, are silicates present in the mafic and ultramafic rocks. They are divided in two different subgroups: the orthopyroxenes which are solid solution with the general formula $(X, Y)_2Si_2O_6$ with X and Y cations being Fe^{2+} and Mg^{2+} and the clinopyroxenes which are solid solution of the general formula XYZ_2O_6 where X have larger cation sites than Y ones such as Na^+ or Ca^{2+}. Z represents the tetrahedral sites; in the case of pyroxene, they are occupied by Si^{4+} and their substitution by Al^{3+} is limited. Orthopyroxenes are defined by two pure endmembers: ferrosilite ($Fe_2Si_2O_6$) and enstatite ($Mg_2Si_2O_6$). Clinopyroxenes are defined by several endmembers: two sodic with jadeite ($NaAlSi_2O_6$) and aegirine ($NaFe^{3+}Si_2O_6$) and a calcic one with wollastonite ($Ca_2Si_2O_6$) being the pure calcic pole. As for olivines, solid solutions between these poles are often observed with diopside (Fe < 50 mol% and 45 < Mg < 50 mol%), hedenbergite (Fe > 50 mol% and 45 < Ca < 50 mol%), augite (20 < Ca < 45 mol% *i.e.*, high-Ca pyroxene) or pigeonite (5 < Ca < 20 mol% *i.e.*, low-Ca pyroxene). If we consider, the redox potential of these pyroxenes, orthopyroxenes and especially ferrosilite appear to have the highest iron content and thus the highest H_2 potential.

Associated with other phases such as plagioclase in basalts, rich in calcium and aluminum, pyroxenes, instead of serpentinization, will undergo a chloritization and amphibolitization reactions depending on the temperature. Secondary minerals will be tremolite, chlorite, talc, hornblende and epidote (Plumlee, 1999). In contrary to serpentinization, these reactions will not produce, directly, high H_2 content.

Amphiboles

Amphiboles are very usual minerals of plutonic and metamorphic rocks. They are double-chain (SiO_4 tetrahedra) silicates. The general formula is $AB_2C_5T_8O_{22}(OH)_2$ where site A (octahedral) can be K or Na; site B (octahedral) can be Na, Ca, Mg, Fe^{2+}, Mn^{2+}, Li, Zn, Ni, and Co; site C (octahedral) can be Al, Fe^{3+}, Mn^{3+}, Cr, Ti, Zr, Zn, Ni, and Co; and site T (tetrahedral) can be Si, Al, and Ti (Leake *et al.*, 1997).

Amphiboles can be categorized in different groups: calcic, sodic, calco-sodic or ferro-magnesio-amphiboles. Substitution between Mg and Fe are very common in amphiboles (Deer *et al.*, 2013) and therefore can be of primary interest in the study of H_2. As the groups of amphiboles are too large, we will focus mainly on the main observed Fe^{2+}-rich amphiboles. It is the case for grunerite $(Fe^{2+},Mg,Mn)_7(Si_8O_{22})(OH)_2$ when $Fe^{2+} > Mg$, which is a common mineral from metamorphosed banded ironstones and in silicic volcanic rocks and can be rich up to 45% of Fe^{2+} (ox%) (Klein, 1964). There is also anthophyllite $(Mg,Fe^{2+})_7(Si_8O_{22})(OH)_2$; ferrohornblende $(Ca_2Fe_4Al)(Si_7AlO_{22})(OH)_2$; actinolite $Ca_2(Mg,Fe^{2+})_5Si_8O_{22}(OH)_2$ with an unusal ferroactinolite; glaucophane $Na_2(Mg,Fe^{2+})_3Al_2(Si_8O_{22})(OH)_2$ to riebeckite $Na_2(Fe^{2+},Mg)_3Fe^{3+}{}_2(Si_8O_{22})(OH)_2$ (Deer *et al.*, 2013).

These amphiboles carry Fe^{2+} and can therefore be altered into a Fe^{3+}-rich phase. This is the case of the sodic amphibole arfvedsonite that can be altered into aegirine in peralkaline granites, which is one hypothesis for the presence of H_2 associated to peralkaline granites (Truche *et al.*, 2021):

$$3Na_3Fe^{2+}{}_4Fe^{3+}Si_8O_{22}(OH)_2 + 2H_2O = 9NaFe^{3+}Si_2O_6 + 2Fe^{2+}Fe^{3+}{}_2O_4 + 6SiO_2 + 5H_2. \quad (A.2)$$

Phyllosilicates

Phyllosilicates are composed of tetrahedral and octahedral sheets. Each tetrahedra are made of one cation T (Si^{4+}, Al^{3+}, and Fe^{3+}), linked to four oxygen atoms. Three of them are shared with adjacent tetrahedra and form a hexagonal mesh pattern. Each octahedra are made of a cation O (Fe^{2+}, Mg^{2+}, Al^{3+}, and Fe^{3+}) linked to 6 oxygen atoms. Octahedron are linked to others by sharing edges. Tetrahedra and octahedra are linked together by sharing a common plane. These characteristics are used to differentiate three categories of phyllosilicates: 1:0 layer or TO clay minerals such as kaolinite and serpentine, 2:1 layer or TOT clay minerals such as micas, smectite or talc, 2:1:1 layer or TOTO clay minerals such as chlorite (Bergaya and Lagaly, 2013).

Serpentines of ideal composition $(Mg,Fe)_3Si_2O_5(OH)_4$ are 1:1 trioctoahedral layer minerals (Bergaya and Lagaly, 2013). Mg-rich serpentine such as lizardite, antigorite, and chrysotile have been highly studied during the past

decades as they are produced by serpentinization. When coupled to water reduction, it produces H_2 and ferric iron is then incorporated to magnetite and serpentine in variable proportions (A.1) depending on the initial iron content of the primary phase (Shervais *et al.*, 2005). Greenalite and cronstedtite are the iron-rich serpentines with the formula being respectively $(Fe^{2+},Fe^{3+})_{2\text{-}3}Si_2O_5(OH)_4$ and $Fe^{2+}{}_2Fe^{3+}(Si,Fe^{3+})_2O_5(OH)_4$. In that sense, serpentine is a marker of hydrogen past and/or present production. The optimum for serpentinization, and thus to H_2 production, occurs at 320 °C.

Smectites are 2:1 dioctahedral $M^+{}_{x+y}(R^{3+}{}_{2\text{-}y}R^{2+}{}_y)(Si_{4\text{-}x}Al_x)O_{10}(OH)^2 \cdot nH_2O$ or trioctahedral $M^+{}_{x+y}(R^{2+}{}_{3\text{-}y}R^+{}_y)(Si_{4\text{-}x}Al_x)O_{10}(OH)_2 \cdot nH_2O$ layer minerals (x, y being the layer charge resulting from tetrahedral and octaedral sites, R^{2+} and R^{3+} being the divalent and trivalent octahedral cations, and M^+ being the monovalent interlayer cation). Interlayer cation are commonly Na^+, K^+, Ca^{2+}, and Mg^{2+} ions. Fe^{2+}, Mg^{2+}, Al^{3+}, and Fe^{3+} ions commonly occupy octahedral sites. The iron-rich smectite is the dioctahedral nontronite with the following structural formula $(Na_{0.3}Fe^{3+}{}_2(Si,Al)_4O_{10}(OH)_2 \cdot nH_2O$. Smectites are known to form under a wide range of conditions from subsurface weathering to hydrothermal conditions.

Micas are 2:1 dioctahedral $(R^+R^{3+}{}_2)(Al,Si)_4O_{10}(OH,F)_2$ or trioctahedral $(R^+R^{2+}{}_3)(Al,Si)_4O_{10}(OH)_2$ layer minerals. Biotite, with the following structural formula $K(Mg,Fe)_3(AlSi_3O_{10})(OH)_2$, is the most common mica and is commonly found in acid and intermediate rocks, such as granites. They are formed under magmatic conditions. During the alteration of these granites, it is the biotite that allows the release of Fe^{2+} into the solution allowing the formation of magnetite, hematite, and iron-rich clay minerals (Murray *et al.*, 2020). In acid rocks, biotites and some amphiboles are the only Fe^{2+} carriers, and are the one to look for. Annite is the iron-rich trioctahedral micas with the structural formula being $KFe^{2+}{}_3(AlSi_3O_{10})(OH)_2$.

Chlorites are usually 2:1:1 trioctahedral layer minerals with Fe^{2+}, Mg^{2+}, Al^{3+}, and Fe^{3+} ions on octahedral sites. Si^{4+}, Al^{3+} are found on the tetrahedral sites, and can be replaced in some specific case by Fe^{3+}. An ideal composition could be expressed as the following one: for the 2:1 layer $(R^{2+}R^{3+})_3(Si,Al)_4O_{10}(OH)_2$ and for the interlayer $(R^{2+}R^{3+})_3(OH)_6$. The iron-rich chlorite is the trioctahedral chamosite with the following structural formula $(Fe^{2+})_5Al(Si_3Al)O_{10}(OH)_8$. Chlorite is a common phyllosilicate of weathering rocks. It is found in acid, intermediate, and basic rocks. In that sense it can be considered as an alteration product and as a temperature marker in the rocks of the oceanic crust and geothermal systems as it becomes dominant between 180 °C and 350 °C (Cathelineau, 1988; Inoue *et al.*, 2010). Chlorites are mainly composed of aluminium, magnesium, and ferrous iron, but redox reaction can occur, and ferric iron can be incorporated to the chlorite formula.

At certain temperature conditions, natural and instantaneous reactions occur within the chlorite itself: dehydrogenation and dihydroxylation. The first is of major interest in this generation of H_2. Its reaction optimum, for a chamosite, is between 390 °C and 410 °C for a transformation of Fe^{2+} into Fe^{3+} up to 70% (Lempart *et al.*, 2018; Steudel *et al.*, 2016).

Thus, chlorite such as serpentine can be considered a past and/or present marker of hydrogen production.

$$\left(Mg,Fe^{2+}\right)_5Al(Si_3Al)O_{10}(OH)_8 \rightarrow \left(Mg,Fe^{3+}\right)_5Al(Si_3Al)O_{10}(OH)_6O_2 + 2H_2. \quad (A.3)$$

Carbonates

Although few studies demonstrated in the past that the alteration of siderite ($FeCO^3$) can lead to the formation of H_2 and CH_4 through a possible reaction presented in equation (A.4) (Milesi *et al.*, 2016), interest of the scientific community concerning Fe-carbonates remained limited until recently. However, late identification of SCDs close to Banded Iron Formations as well as gold mineralization that are Fe-carbonate rich, definitely launched the debate on the true generation potential of this class of minerals (Boreham *et al.*, 2021; Geymond *et al.*, 2022). Preliminary thermodynamic calculations suggested that siderite is a good H_2 generator at $T < 200$ °C, validating that it is worth to study further this kind of minerals (Malvoisin and Brunet, 2023).

$$3Fe^{2+}CO_3 + H_2O \rightarrow Fe^{2+}Fe^{3+}{}_2O_4 + 3CO_2 + H_2. \quad (A.4)$$

Oxides

Fe-oxide are known for years to play a key-role in H_2 generation since magnetite (α-Fe_3O_4) incorporates Fe^{3+} during serpentinization of basic rocks at $T > 200$ °C (Tutolo *et al.*, 2020). As such, the presence of magnetite in basic rocks, even if they can be of primary origin, is often used as a proxy to evaluate the rate of serpentinization and thus the H_2 generation (Malvoisin *et al.*, 2012). Magnetite, like other spinel type minerals such as chromite ($FeCr_2O_4$), are also thought to catalyze H_2 generation during water-rock reactions, for instance during the serpentinization, or conversion of H_2 into CH_4 through the Sabatier's reaction (Mayhew *et al.*, 2013).

In parallel, the fact that a remnant of Fe^{2+} is present in magnetite (1/3 of total Fe theoretically) recently raised questions about its potential to generate H_2 related to further grade of Fe oxidation. A recent experimental study demonstrated that magnetite gets destabilized in anoxic water, following the equation (A.5), to form H_2 and maghemite (γ-Fe_2O_3), another Fe-oxide only bearing Fe^{3+} (Geymond *et al.*, 2023), especially below 100 °C. Magnetite is present as a major component in many rocks, and these results widen the potential source rock that could generate H_2 (Geymond *et al.*, 2022). Banded Iron Formations, very rich in magnetite, are now considered as a possible H_2 generating rock.

$$2\left(\alpha - Fe^{2+}Fe^{3+}{}_2O_4\right) + H_2O \rightarrow 3\left(\gamma - Fe^{3+}{}_2O_3\right) + H_2. \quad (A.5)$$

Sulphides

Ferrous iron sulphide, like pyrrhotite, is widely present in the hydrothermal systems of basic rocks and pegmatites. It is often found in association with other sulphides such as pyrite and chalcopyrite. It is of interest in the production of H_2, which this time does not involve the reduction of water but the oxidation of H_2S gas. This reaction often occurs in volcanic hydrothermal settings. Thus, pyrite is a potential marker mineral for H_2 production, if the geological context is suitable. Here is the example of the alteration of troilite into pyrite associated to the formation of H_2:

$$FeS + H_2S \rightarrow FeS_2 + H_2. \quad (A.6)$$

References of Appendix A

Bergaya F., Lagaly G. (2013) Chapter 1 – general introduction: clays, clay minerals, and clay science, in: Bergaya F., Lagaly G. (eds), Handbook of clay science: Developments in clay science, Elsevier, pp. 1–19. https://doi.org/10.1016/B978-0-08-098258-8.00001-8.

Boreham C.J., Edwards D.S., Czado K., Rollet N., Wang L., Van der Wielen S., Champion D., Blewett R., Feitz A., Henson, P. A. (2021) Hydrogen in Australian natural gas: occurrences, sources and resources, *APPEA J.* 61, 1, 163. https://doi.org/10.1071/AJ20044.

Cathelineau M. (1988) Cation site occupancy in chlorites and illites as a function of temperature, *Clay Miner.* 23, 4, 471–485. https://doi.org/10.1180/claymin.1988.023.4.13.

Deer W.A., Howie R.A., Zussman J. (2013) An Introduction to the Rock-Forming Minerals, 3 edn. The Minerological Society, London, 498 p.

Geymond U., Ramanaidou E., Lévy D., Ouaya A., Moretti I. (2022) Can weathering of banded iron formations generate natural hydrogen? Evidence from Australia, Brazil and South Africa, *Minerals* 12, 2, 163. https://doi.org/10.3390/min12020163.

Geymond U., Briolet T., Combaudon V., Sissmann O., Martinez I., Duttine M., Moretti I. (2023) Reassessing the role of magnetite during natural hydrogen generation, *Front. Earth Sci.* 11, 1169356. https://doi.org/10.3389/feart.2023.1169356.

Inoue A., Kurokawa K., Hatta T. (2010) Application of chlorite geothermometry to hydrothermal alteration in Toyoha geothermal system, Southwestern Hokkaido, Japan, *Resour. Geol.* 60, 1, 52–70. https://doi.org/10.1111/j.1751-3928.2010.00114.x.

Klein F., Bach W., Mccollom T.M. (2013) Compositional controls on hydrogen generation during serpentinization of ultramafic rocks, *Lithos* 178, 55–69. https://doi.org/10.1016/j.lithos.2013.03.008.

Klein J.C. (1964) Cummingtonite-grunerite series: a chemical, optical and X-ray study, *Am. Miner. J. Earth Planet. Mater.* 49, 7–8, 963–982.

Leake B.E., Woolley A.R., Arps C.E., Birch W.D., Gilbert M.C., Grice J.D., Hawthorne F.C., Kato A., Kisch H.J., Krivovichev V.G., Linthout K., Laird J., Mandarino J., Maresh W.V., Nickel E.H., Rock N.M.S., Schumacher J.C., Smith D.C., Stephenson N.C.N., Ungaretti L., Whittaker E.J.W., Youzhi G. 1997. Nomenclature of amphiboles report of the Subcommittee on Amphiboles of the International Mineralogical Association Commission on New Minerals and Mineral Names, *Can. Mineral.* 35, 1, 219–246.

Lempart M., Derkowski A., Luberda-Durnaś K., Skiba M., Bõõlachowski A. (2018) Dehydrogenation and dehydroxylation as drivers of the thermal decomposition of Fe-chlorites. *Am. Mineral.* 103, 11, 1837–1850. https://doi.org/10.2138/am-2018-6541.

Malvoisin B., Brunet F. (2023) Barren ground depressions, natural H2 and orogenic gold deposits: Spatial link and geochemical model. *Sci. Total Environ.* 856, 158969. https://doi.org/10.1016/j.scitotenv.2022.158969

Mayhew L.E., Ellison E.T., McCollom T.M., Trainor T.P., Templeton, A.S. (2013) Hydrogen generation from low-temperature water–rock reactions, *Nat. Geosci.* 6, 6, 478–484. https://doi.org/10.1038/ngeo1825

Milesi V., McCollom T.M., Guyot F. (2016) Thermodynamic constraints on the formation of condensed carbon from serpentinization fluids, *Geochim. Cosmochim. Acta* 189, 391–403. https://doi.org/10.1016/j.gca.2016.06.006.

Murray J., Clément A., Fritz B., Schmittbuhl J., Bordmann V., Fleury J.M. (2020) Abiotic hydrogen generation from biotite-rich granite: A case study of the Soultz-sous-Forêts geothermal site, France, *Appl. Geochem.* 119, 104631. https://doi.org/10.1016/j.apgeochem.2020.104631.

Plumlee G.S. (1999) The environmental geology of mineral deposits, in: Plumlee G.S., Logdson M.J. (eds), The environmental geochemistry of mineral deposits, part A. Processes, techniques and health issues, Littleton, CO, USA, pp. 71–116.

Shervais J.W., Kolesar P., Andreasen K. (2005) A field and chemical study of serpentinization – Stonyford, California: chemical flux and mass balance, *Int. Geol. Rev.* 47, 1, 1–23. https://doi.org/10.2747/0020-6814.47.1.1.

Steudel A., Kleeberg R., Koch C.B., Friedrich F., Emmerich K. (2016) Thermal behavior of chlorites of the clinochlore-chamosite solid solution series: oxidation of structural iron, hydrogen release and dehydroxylation, *Appl. Clay Sci.* 132–133, 626–634. https://doi.org/10.1016/j.clay.2016.08.013.

Truche, L., Bourdelle, F., Salvi, S., Lefeuvre, N., Zug, A., Lloret, E. (2021) Hydrogen generation during hydrothermal alteration of peralkaline granite, *Geochim. Cosmochim. Acta* 308, 42–59. https://doi.org/10.1016/j.gca.2021.05.048.

Tutolo B.M., Seyfried W.E., Tosca N.J. (2020) A seawater throttle on H2 production in Precambrian serpentinizing systems, *Proc. Natl. Acad. Sci.* 117, 26, 14756–14763. https://doi.org/10.1073/pnas.1921042117.

Appendix B

Coordinates of the sites discussed in the paper and of the pictures from the fieldworks.

Figure	Country	Latitude	Longitude
Figure 3a	Republic of Djibouti	11.5461	42.4782
Figure 3c	Bolivia	−22.4311	−67.7584
Figure 3d	Italy	43.0819	11.8023
Figure 3e	Australia	−37.0399	141.2982
Figures 3g and 3h	Namibia	−25.6895	16.8285
Figure 4	Brazil	−16.5592	−45.3436
Figures 5a and 5b	Namibia	−29.0564	17.1283
Figures 5c and 5d	Namibia	−24.2935	18.0308
Figure 7	Russia	51.2113	42.01664
Figures 10a and 10b	Namibia	−20.6274	17.4667
Figure 11	Turkey	36.4314	30.4561
Figures 12a and 12b	Namibia	−21.2194	18.0402

Appendix C

Analytical tools to study a rock H_2 potential with their characteristics.

Analyses	Objectives	Limitations	Spatial resolution	Limit of detection	Sample type	Duration of preparation/analysis/processing
Bulk characterization						
Rock-Eval	Characterization of the Total Organic Content (TOC) Access to mineral and organic contents but also thermal analysis of C and S				Powder (~10 mg)	min/min/min
X-ray fluorescence	Major elements concentrations (Fe, S, U, Th, K)	Does not detect trace elements	–	Depends on the element	Soli, powder, liquid	–/min/min
Inductively Coupled Plasma – Mass Spectrometry/Optical Emission Spectroscopy (ICP-MS/OES)	Majors, minors, traces, and ultra-traces concentrations (Fe, S, U, Th, K)			ppb	Powder (~100 mg)	hours/hours/days
^{57}Fe Mössbauer spectroscopy	Identification and quantification of iron-bearing phases and iron specification in each phase				Powder (~400 mg)	hours/days/days
X-Ray Diffraction	Phase identification, quantitative composition	Do not differentiate polymorphs or minor phase	–		Powder (~500 mg)	hours/hours/hours
Observation tool						
Optical microscopy	Paragenesis, texture, alteration features	Low resolution	µm	–	Thin section	
Electro Probe Micro-Analyzer (EPMA)	Quantitative measurements of concentration of the element heavier than Li (Fe, S, U, Th, K) punctual or map		µm	ppm	Thin section	hours/day(s)/days

(Continued on next page)

(Continued)

Analyses	Objectives	Limitations	Spatial resolution	Limit of detection	Sample type	Duration of preparation/analysis/ processing
Scanning Electron Microscopy (SEM)	High-resolution imaging demi-quantitatve measurements of concentration of the element heavier than Li (Fe, S, U, Th, K) punctual or map	Semi-quantitative	nm	–	Thin section	hours/hours/hours
Raman Microspectroscopy	Phase identification		µm		Thin section	hours/days/days
X-Rays Microtomography (XCT)	Volume and propagation of elements of interest-bearing phase in the whole rock	No chemical information, can be hard to distinguish chemically close phases, post-processing can be challenging, time consuming	µm		cm^3–m^3 core	hours/hours/days